Journal of Nanobiotechnology

https://doi.org/10.1186/s12951-025-03943-5

Article in Press

Bidirectional regulation of liver sinusoidal clearance by amino acid nanofibers and IGFBP4 complex: effects on HbA1c

Received: 14 August 2025

Accepted: 13 December 2025

Published online: 26 December 2025

Cite this article as: Lee A., Castelli S.d.L., Sellers P. *et al.* Bidirectional regulation of liver sinusoidal clearance by amino acid nanofibers and IGFBP4 complex: effects on HbA1c. *J Nanobiotechnol* (2025). https://doi.org/10.1186/s12951-025-03943-5

Aejin Lee, Silvia de Lamo Castelli, Patrick Sellers, Sagarika Taneja, Mayreli Ortiz, Devan Kowdley, Jacob H. Leung, Binod Pokharel, Latha P. Ganesan, Bradley J. Needleman, Sabrena F. Noria, Luis Rodriguez-Saona, Lianbo Yu, Jon R. Parquette & Ouliana Ziouzenkova

Bidirectional Regulation of Liver Sinusoidal Clearance by Amino Acid Nanofibers and IGFBP4 Complex: Effects on HbA1c

Aejin Lee[1,2,† [0000-0001-7780-4961]], Silvia de Lamo Castelli[3,4,†[0000-0002-5261-6806]], Patrick Sellers[1,† [0009-00030-4779-3001]], Sagarika Taneja[5 [0009-0002-8745-5915]], Mayreli Ortiz[4 [0000-0002-9423-0055]], Devan Kowdley[1], Jacob H. Leung[1], Binod Pokharel[1 [0009-0005-8962-4788]], Latha P. Ganesan[8[0000-00025-4236-6620]], Bradley J. Needleman[6], Sabrena F. Noria[7] , Luis Rodriguez-Saona[3[0000-0002-6615-1296]], Lianbo Yu[9 [0000-0002-2025-2585]], Jon R. Parquette[5 [0000-0002-4803-028X]], and Ouliana Ziouzenkova [1,* [0000-0003-2449-2591]]

[1] Department of Human Sciences, The Ohio State University, Columbus, Ohio, 43210, USA.; ajlee@mju.ac.kr (A.L.); sellers.242@buckeyemail.osu.edu (P.S.); kowdley.2@buckeyemail.osu.edu (D.K.); leung.167@buckeyemail.osu.edu (J. H. L.); pokharel.18@buckeyemail.osu.edu (B.P.); Ziouzenkova.1 @osu.edu (O.Z.)

[2] Food and Nutrition Major, Division of Integrative Biosciences, Myongji University, Yongin, 17058, Republic of Korea; ajlee@mju.ac.kr (A.L.)

[3] Department of Food Ag Biological Engineering, The Ohio State University Columbus, OH 43210-1007, USA: delamocastellvi.1@osu.edu (S.d.L.C.); guduru.4@osu.edu (S.G.); rodriguez-saona.1@osu.edu (L.R.S.)

[4] Universitat Rovira i Virgili, Departament d'Enginyeria Química, Food Innovation & Engineering Group, Av. Països Catalans 26, Campus Sescelades, 43007 Tarragona, Spain; silvia.delamo@urv.cat (S.d.L.C.); mayreli.ortiz@urv.cat (M.O.)

[5] Department of Chemistry and Biochemistry, The Ohio State University, Columbus, Ohio, 43210, USA; taneja.33@buckeyemail.osu.edu (S.T.); parquette.1@osu.edu (J. R . P)

[6] Comprehensive Weight Management & Bariatric Surgery Center, The Ohio State University Wexner Medical Center, The Ohio State University, Columbus, Ohio, 43210, USA; bradley.needleman@osumc.edu (B.J.D.)

[7] Division of General and Gastrointestinal Surgery, The Ohio State University Wexner Medical Center, The Ohio State University, Columbus, Ohio, 43210, USA; sabrena.noria@osumc.edu (S.F.N.)

[8] Department of Internal Medicine, The Ohio State University Wexner Medical Center, The Ohio State University, Columbus, Ohio, 43210, USA; latha.ganesan@osumc.edu (L.P.G.)

[9] Department of Biomedical Informatics, The Ohio State University, Columbus, Ohio, 43210, USA; lianbo.yu@osumc.edu (L.Y.)

* Correspondence: ziouzenkova.1@osu.edu; Tel.: 001 614 292 5034

† These authors contributed equally to this work.

Abstract.

Therapies for type 2 diabetes primarily target hyperglycemia; however, complications are also triggered by advanced glycation end products (AGEs). We hypothesize that the anti-diabetic efficacy of insulin-like growth

factor-binding protein 4 (IGFBP4) is enhanced when it assembles with a specific amino acid compound-2 (AAC2) into nanostructures. Their effects were examined in vitro and in *ob/ob* mice treated for 30 days with the AAC2–IGFBP4 complex or its individual components. IGFBP4-mediated glucose uptake in human and mouse preadipocytes was enhanced by complex formation with AAC2, as confirmed by Fourier-transform mid-infrared spectroscopy, electrophoresis, and AFM. In *ob/ob* mice, the complex prolonged IGFBP4 circulation and amplified the effects of the individual components, resulting in reduced hyperphagia, body weight, and hyperinsulinemia, along with improved insulin sensitivity and glucose tolerance. Notably, HbA1c levels remained at 5.9% in the complex-treated group compared to >7% in others, with lower plasma AGE levels than in AAC2-treated mice. Transcriptomic and pathway analyses revealed that the complex upregulated genes promoting the fenestrated phenotype of liver sinusoidal endothelial cells (LSECs), facilitating AGE and waste clearance, whereas free AAC2 inhibited this process. We propose a 'scavenger-input' hypothesis in which free AAC2 inhibits, while the AAC2–IGFBP4 complex activates fenestrated phenotype and waste-clearance capacity in liver sinusoidal endothelial cells (LSECs). Based on our results, AAC2 could serve as an adaptable and inherently therapeutic nanofiber modality that enhances the functional properties of bound proteins, offering multidimensional treatment possibilities for diabetes and other degenerative disorders.

Keywords: liver sinusoidal system, drug clearance, toxins removal, TGFβ, HbA1C

Graphic abstract

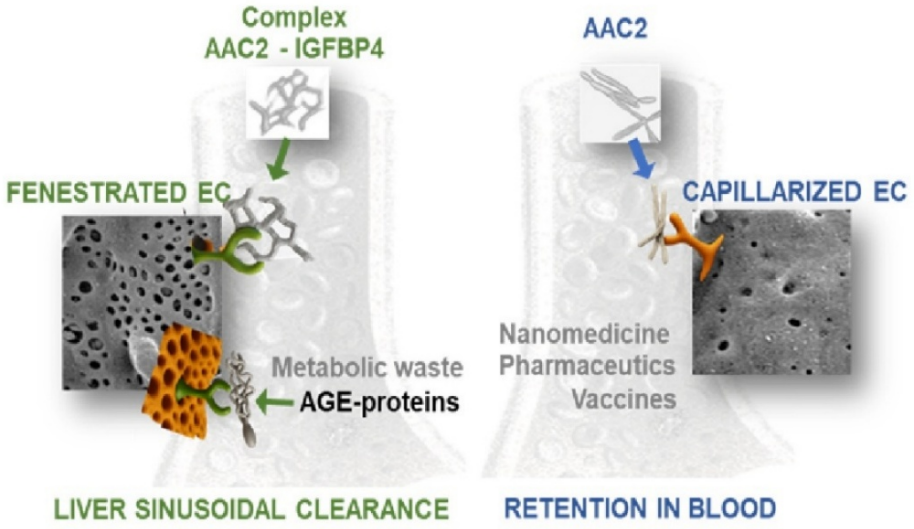

Schematics 1. Advanced glycation end product (AGE) clearance from the blood is regulated by AAC2 nanofibers and their interaction with IGFBP4. The AAC2–IGFBP4 complex promotes a fenestrated phenotype in liver sinusoidal endothelial cells (LSECs), thereby enhancing the clearance of AGEs and other circulating waste products. In contrast, free AAC2 nanofibers exert the opposite effect, inducing LSEC capillarization and consequently limiting the clearance of pharmaceuticals, nanotherapeutics, vaccines, AGEs, and additional metabolic and inflammatory by-products. The biological activity of AAC2 depends on leptin receptor signaling, whereas the AAC2–IGFBP4 complex activates gene programs associated with endothelial fenestration and clearance capacity, correlating with increased expression of the stabilin-2 and Fcgr2b clearance receptors.

1 Introduction

The debilitating consequences of type 2 diabetes mellitus (T2DM) continue to pose a major public health challenge [1], ranking as the fourth leading cause of disability-adjusted life years [2]. Although the treatment of hyperglycemia remains a cornerstone of T2DM management, hospitalizations for hyperglycemic crises have steadily increased over the past two decades following a period of decline [2]. T2DM is associated with both microvascular and macrovascular complications [2, 3] and affects multiple organs, including the kidneys (diabetic nephropathy), heart (diabetic cardiomyopathy), and liver (non-alcoholic steatohepatitis and fibrosis) [4]. These complications are characterized by chronic inflammation and progressive fibrosis, ultimately leading to organ dysfunction and failure [5]. While hyperglycemia remains the primary therapeutic target for most anti-diabetic drugs [6], the accumulation of advanced glycation end products (AGEs), derived from reactive carbonyl species such as methylglyoxal (MGO) [7], has been implicated in irreversible protein modifications [8] and the development of vascular complications in T2DM [3]. Multifactorial approaches targeting both hyperglycemia and AGE clearance may be essential for advancing the treatment of T2DM complications.

Both hyperglycemia and AGEs contribute to the formation of glycated hemoglobin (HbA1c), a clinical marker used to assess long-

term glucose control and predict the risk of complications [9]. AGEs activate the receptor for AGE (RAGE), initiating a pro-inflammatory cascade through pathways such as NF-κB and MAPK/ERK, which upregulate inflammatory cytokines and exacerbate oxidative stress [10]. This inflammatory environment promotes the activation of the TGFβ pathway and induces IL-11 expression, establishing a feedforward loop that worsens tissue injury, fibrosis, and results in ceased functioning [11]. An alternative mechanism for AGE clearance involves the liver sinusoidal endothelial cells (LSEC), which express the type H scavenger receptors stabilin-1 and stabilin-2 [12]. Besides AGEs, these receptors facilitate the removal of various waste products, including lipopolysaccharide (LPS), thereby mitigating systemic inflammation [13, 14]. Deficiency in these receptors has been linked to glomerulofibrotic nephropathy, fibrosis, and premature mortality [15], although their role in diabetic complications [16] remains underexplored.

Nanotechnology-based interventions offer promising therapeutic alternatives by tar-geting both hyperglycemia and its underlying pathogenic mechanisms. Artificial nano-fibers such as AAC2, which act as atypical ligands for the leptin receptor (LepR), have been shown to modulate metabolic pathways [17, 18]. AAC2 activates LepR and atypical protein kinase C zeta, thereby enhancing glucose uptake in insulin-insensitive tissues [18]. Moreover, AAC2 forms

stable nanofiber complexes with insulin, extending insulin's half-life in circulation and improving both glycemic control and cognitive function in diabetic models by balancing anabolic and catabolic signaling through insulin and leptin receptors [17]. Despite these advances, the molecular interactions between AAC2 and endogenous regulators of glucose metabolism beyond insulin [17] remain poorly understood, representing a critical knowledge gap in the development of next-generation anti-diabetic therapeutics.

Insulin-like growth factor binding protein 4 (IGFBP4) has recently been identified as one of five critical biomarkers of biological aging [19]. IGFBP4 is the most abundant member of the IGFBP family of six structurally related proteins [20]. IGFBP4 is secreted by multiple tissues, including myocytes [21] and all adipocyte subtypes [22]. Its secretion is particularly enhanced in thermogenic *Aldh1a1*$^{-/-}$ adipocytes, which exhibit high glucose uptake [23, 24]. The best-characterized role of IGFBP4 in glucose metabolism involves its binding to insulin-like growth factors IGF-1 and IGF-2 [25]. Proteolytic cleavage of the IGFBP4–IGF-1 complex (holo-IGFBP4) near the cell surface leads to IGF-1 release and a transient surge in glucose uptake [26]. The sequestration of IGF-1 by IGFBP4 is significant, as low IGF-1 levels have been associated with increased longevity in humans and animal models [27].

Evidence suggests that proteolytic fragments of IGFBP4 accelerate atherosclerosis, particularly in individuals with diabetes [28], while a mutated form of IGFBP4 resistant to proteolysis improves cardiac recovery following acute myocardial infarction [29]. In its non-liganded form (apo-IGFBP4), the protein resists proteolytic cleavage and functions as a cardiogenic growth factor inhibiting the assembly of Wnt3a with Frizzled-8 and LRP6 [21], where LRP6 has also been implicated in the regulation of glucose metabolism [30]. However, the role of apo-IGFBP4 in models of hyperglycemia, glucose intolerance, and insulin resistance has not been investigated.

AAC2 binding protects insulin in circulation [17], acting as a scaffold that may also modulate clearance of IGFBP4, the dynamics between IGFBP4 and its IGF-1-bound complex, and proteolytic degradation of this complex. Therefore, the current study aims to investigate the effects of IGFBP4 alone or in complex with AAC2 in *ob/ob* mice, a well-established model of insulin resistance, hyperglycemia, and leptin deficiency [31]. By characterizing this interaction, we seek to define IGFBP4's function in T2DM and determine whether synthetic nanomaterial AAC2 can enhance the therapeutic potential of IGFBP4.

2 Results

2.1 The AAC2–IGFBP4 combination enhances glucose uptake and amplifies the anti-inflammatory effects of its individual components in vitro

We investigated the properties of the apo-form of human IGFBP4 (hIGFBP4, UniProt ID: P22692; **Fig. 1a**). In apo-IGFBP4, the cysteine-rich N- and C-terminal domains are unoccupied by IGF1 or IGF2 [32], exposing electronegative and hydrophobic regions that may facilitate interactions with other molecules. Here, we examined the potential interaction between hIGFBP4 and the positively charged, hydrophobic AAC2 nanofibers, previously characterized in [18] (**Fig. 1b**). Given that hyperglycemia induces the production of proinflammatory methylglyoxal (MGO), a precursor of advanced glycation end products (AGEs), we also investigated its potential interference with AAC2 and hIGFBP4 (**Fig. 1c**).

We assessed the glycemic effects of hIGFBP4 by measuring glucose uptake in primary human subcutaneous adipocytes isolated from six obese individuals (BMI

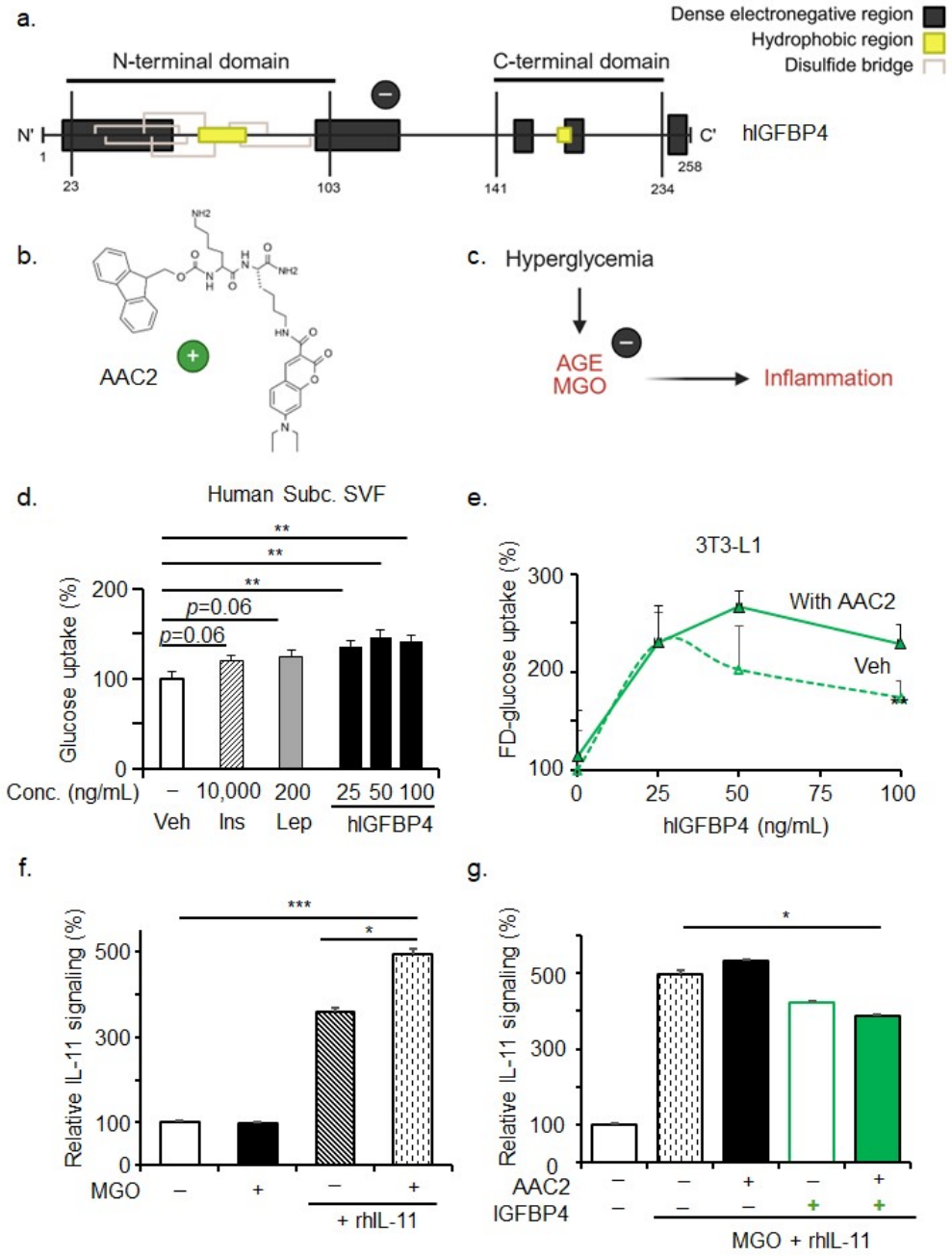

Fig. 1. Combination of apo-hIGFBP4 with electropositive AAC2 nanofibers enhances glucose uptake and attenuates the

proinflammatory effects of MGO. (a) Schematic representation of hIGFBP4 structure highlighting domains susceptible to interaction with charged, hydrophobic, and oxidant molecules. (b) AAC structure: a dilysine backbone modified with a hydrophobic coumarin side group, enabling self-assembly into positively charged nanofibers. (c) Schematic of methylglyoxal (MGO) production under hyperglycemic stress, showing its role as a precursor of electronegative AGEs and driver of diabetic inflammation. (d) FD-glucose uptake in human subcutaneous SVF preadipocytes isolated from obese patients (n = 6) with and without diabetes. Confluent cells were glucose- and serum-deprived (starved) for 40 min and treated with vehicle (Veh, PBS) or designated concentrations of insulin (Ins), leptin (Lep), and hIGFBP4. Statistical analysis was performed using unpaired t-test. *P = 0.05–0.01; **P = 0.01–0.001; ***P < 0.001. (e) Dose-dependent FD-glucose uptake in 3T3-L1 preadipocytes (n = 4) starved for 50 min and treated for 90 min with hIGFBP4 alone or with AAC2 (0.1 µM). (f) IL-11 reporter activity in HEK293 cells (n = 4) after 24 h stimulation with recombinant human IL-11 (1 ng/mL), MGO (10 µM), or their combination. Data is expressed as a percentage relative to unstimulated control. (g) HEK293 cells (n = 4) were stimulated for 24 h with IL-11 and MGO (as in panel f) in the presence or absence of AAC2 (1 µM), hIGFBP4 (50 ng/mL), or their combination.

50.4 ± 6.67; Table S1) with and without T2D (HbA1c 5.82 ± 0.75), in comparison to insulin and leptin (**Fig. 1d**). The apo-form of hIGFBP4 increased glucose uptake in a dose-dependent manner in these human adipocytes. Similarly, it enhanced FD-glucose uptake in a

dose-dependent fashion in murine 3T3-L1 preadipocytes (**Fig. 1e**). Notably, the combination of AAC2 and hIGFBP4 significantly increased FD-glucose uptake compared to hIGFBP4 alone at concentrations above 75 ng/mL. To determine whether hIGFBP4 and AAC2 also modulate inflammatory responses, we used human kidney HEK293 reporter cells as a model of feed-forward IL-11-driven fibrotic inflammation relevant to diabetic nephropathy [33]. As expected, IL-11 stimulation increased IL-11 production by 360%, while MGO (10 µM), a concentration consistent with levels in diabetic patients (7 µM) [34, 35], had no effect alone (**Fig. 1f**). However, co-stimulation with IL-11 and MGO resulted in a 500% increase in IL-11 production compared to control and a significant rise relative to IL-11 alone, consistent with MGO-induced glucotoxicity in diabetes [35]. The induction of IL-11 by IL-11 + MGO was not affected by AAC2 or hIGFBP4 alone; however, their combined treatment significantly reduced this proinflammatory response (**Fig. 1g**). Given the enhanced glucose uptake and anti-inflammatory effects of the AAC2–hIGFBP4 combination, along with their electrostatic complementarity, we investigated potential complex formation between these molecules.

2.2 Evidence for Complex Formation Between AAC2 and hIGFBP4

We analyzed AAC2 (1 mM), recombinant human IGFBP4 (hIGFBP4, 10 ng/mL), and a mixture of AAC2 (1 mM) with hIGFBP4 (10 ng/mL), using Fourier-transform mid-infrared spectroscopy [36] to assess differences in secondary protein structure within the 1600–1700 cm^{-1} spectral region via deconvolution analysis [37]. **Fig. 2a** displays relative percentages of side chain vibrations, parallel and antiparallel β-sheet, random coils, α-helix and β-turn of hIGFBP4 and AAC2-hIGFBP4 complex. AAC2-hIGFBP4 complex induced conformational changes resulted in the decrease in parallel β-sheet content, α-helix, random coils content, accompanied by increase in β-turn, anti-parallel β-sheet content at 1689 cm^{-1}, and side chains. This pattern suggests a substantial conformational rearrangement, where flexible regions (random coils [38] are replaced by more ordered β-structures. The increase in β-turns likely facilitates the alignment of strands into antiparallel β-sheets. At the same time, the loss of α-helices and coil structures may indicate structural remodeling that favors the adoption of more stable, antiparallel β-sheet conformations, which are characteristic for complex stabilization [39]. The observed increase inside chain-associated signals (1603–1606 cm^{-1}) may be linked to changes in the local chemical environment of specific amino acid residues or free AAC2.

These shifts may reflect reorientation, altered exposure, or new interactions of side chains upon binding, contributing to the stabilization of the complex through hydrogen bonding, electrostatic attractions, or hydrophobic contacts. Heat treatment of hIGFBP4 (hIGFBP4^{Inact}), altered properties of AAC2-hIGFBP4^{Inact} complex, demonstrating an increase in β-turns (**Fig. 2b**) could be attributed to the loss of stability or dissociation of AAC2 from heat-inactivated hIGFBP4 [40]. These findings indicate a specific interaction between AAC2 and hIGFBP4, which appear to be disrupted upon denaturation of the protein.

Native gel electrophoresis (**Fig. 2c**) further confirmed complex formation, showing that the AAC2-hIGFBP4 complex migrated as a higher molecular weight band compared to free hIGFBP4 and the denatured hIGFBP4 mixture with AAC2. These results validated complex formation in vitro.

The nanofiber structure of AAC2 observed by TEM [18] was further confirmed by Atomic Force Microscopy (AFM) (**Fig. 2d**). AAC2 nanofibers retained their fibrous morphology or appeared to wrap around themselves, likely due to a combination of repulsive electrostatic forces and hydrophobic interactions. AFM also showed that AAC2 interacts with multiple regions of the IGFBP4 protein (white areas), displaying variable binding affinity.

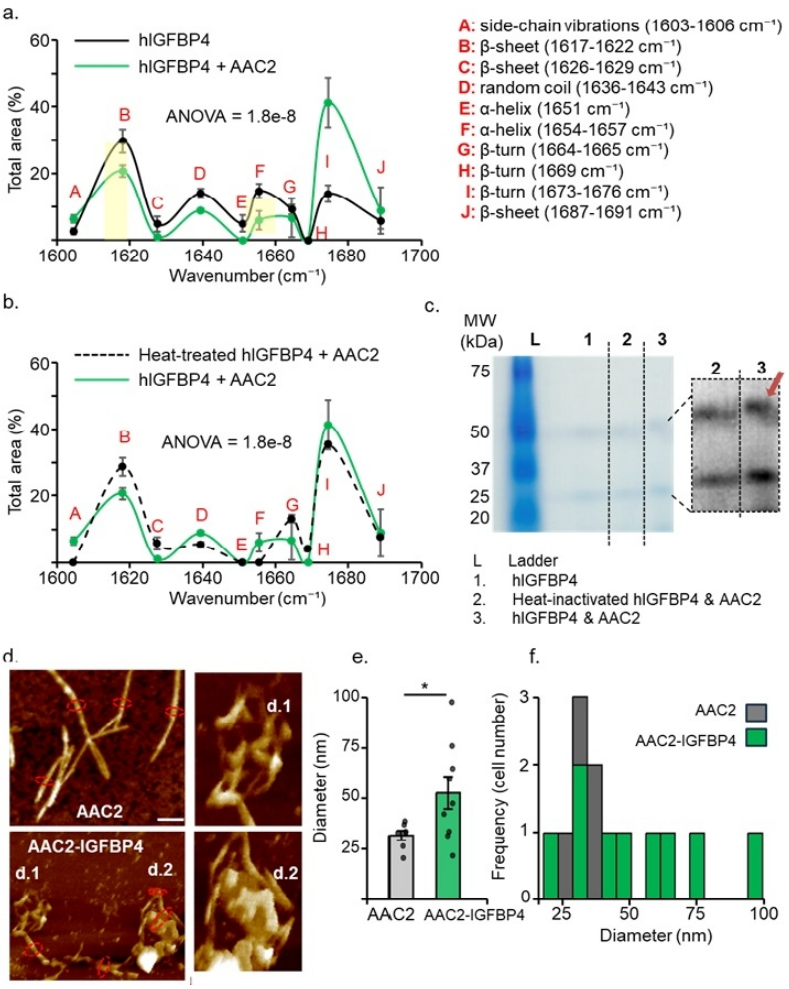

Fig. 2. Apo-hIGFBP4 complex with AAC2 exhibits distinct IR spectral and electrophoretic characteristics. (a) ATR FT-MIR spectra of hIGFBP4 with and without bound AAC2 were analyzed by spectral deconvolution in the 1600–1700 cm^{-1} region. Highlighted are β-sheets, and α-helices. Each sample was measured five or more times and shown as representative samples. Statistical analysis was performed using one-way ANOVA. (b) ATR FT-MIR spectra of AAC2 with native and denatured by heat inactivation

hIGFBP4 analyzed by spectral deconvolution in the 1600–1700 cm^{-1} region. (c) Electrophoresis of hIGFBP4 (lane 1), AAC2 with denatured hIGFBP4 (lane 2), and AAC2 with native hIGFBP4 (lane 3), performed under denaturing conditions. (d) AFM image of AAC2 and the AAC2-IGFBP4 complex, with the enlarged regions shown in inserts d.1 and d.2. (e, f) Fiber diameter measurements (e, indicated by red circles) and corresponding histogram distribution (f) derived from AFM images of AAC2 (n=7) and the AAC2-IGFBP4 complex (n=9, $*P=0.03$).

Unlike AFM images of native or aggregated proteins [41], the electrostatic complementarity between AAC2 and hIGFBP4 may promote the formation of globular and fibrous structures of differing compaction, as illustrated in the enlarged inserts (**Fig. 2d**, panels **d.1** and **d.2**). In agreement with these observations, the diameters of nanofibers measured at randomly selected sites showed considerable variability and were significantly greater in the AAC2–hIGFBP4 complex than in free AAC2 alone (**Fig. 2e**), with large-diameter fibers observed exclusively in the AAC2–hIGFBP4 complex (**Fig. 2f**). The very large diameters (~100 nm) might emerge from bundling instead of a single protein binding. This pattern is consistent with the abundant electronegative and hydrophobic residues present in the N-terminal region of IGFBP4 compared with the central and C-terminal domains.

2.3 Endogenous IGFBP4 and IGF-1 levels are unchanged by AAC2/hIGFBP4 treatment in *ob/ob* mice

The improved glycemic and anti-glucotoxic properties of the AAC2–hIGFBP4 complex observed in vitro prompted us to examine its effects in leptin-deficient, insulin-resistant *ob/ob* male mice (**Fig. 3a**). After acclimation, mice were randomized into four groups with similar body weight and fasting glucose levels and received intrascapular subcutaneous injections of vehicle (Veh, PBS), AAC2 (0.1 nmol/g body weight [BW]),

observed in vitro prompted us to examine its effects in leptin-deficient, insulin-resistant *ob/ob* male mice (**Fig. 3a**). After acclimation, mice were randomized into four groups with similar body weight and fasting glucose levels and received intrascapular subcutaneous injections of vehicle (Veh, PBS), AAC2 (0.1 nmol/g body weight [BW]), hIGFBP4 (1.79 nmol/g BW), or AAC2–hIGFBP4 (0.1 nmol/g and 1.79 nmol/g, respectively) every 48 hours for 30 days. In our previous study, AAC2 binding prolonged the circulation time of therapeutic insulin [17]; therefore, we measured plasma hIGFBP4 concentrations in all treatment groups 48 hours after injection (**Fig. 3b**). Circulating hIGFBP4 was detectable only in mice treated with the AAC2–hIGFBP4 complex, supporting the role of AAC2 nanofibers as a protective scaffold.

Endogenous murine IGFBP4 levels were significantly elevated in *ob/ob* mice treated with either free hIGFBP4 or AAC2–hIGFBP4 compared to controls (**Fig. 3c**). Since IGF-1 is the canonical binding partner of IGFBP4 and plays a role in glucose regulation [42], we compared IGF-1 levels across groups and found no significant differences (**Fig. 3d**). The comparable plasma levels of endogenous IGFBP4 and IGF-1 in both
treatment conditions suggest that these proteins are unlikely to account for the differing
effects of free versus AAC2-bound hIGFBP4.

2.4 AAC2–hIGFBP4 complex, but not free hIGFBP4, reduces body weight and food intake in *ob/ob* mice

Consistent with the known phenotype, *ob/ob* mice in the control (Veh) group gained

Similar weight gain and final body weight were observed in mice treated with free AAC2 or hIGFBP4. However, treatment with the AAC2/hIGFBP4 complex resulted in a moderate reduction in both weight gain (-7.7%) and body weight (–6%) compared to control *ob/ob* mice (100%). These effects were absent in *db/db* mice subjected to similar treatments (**Fig. S1a**).

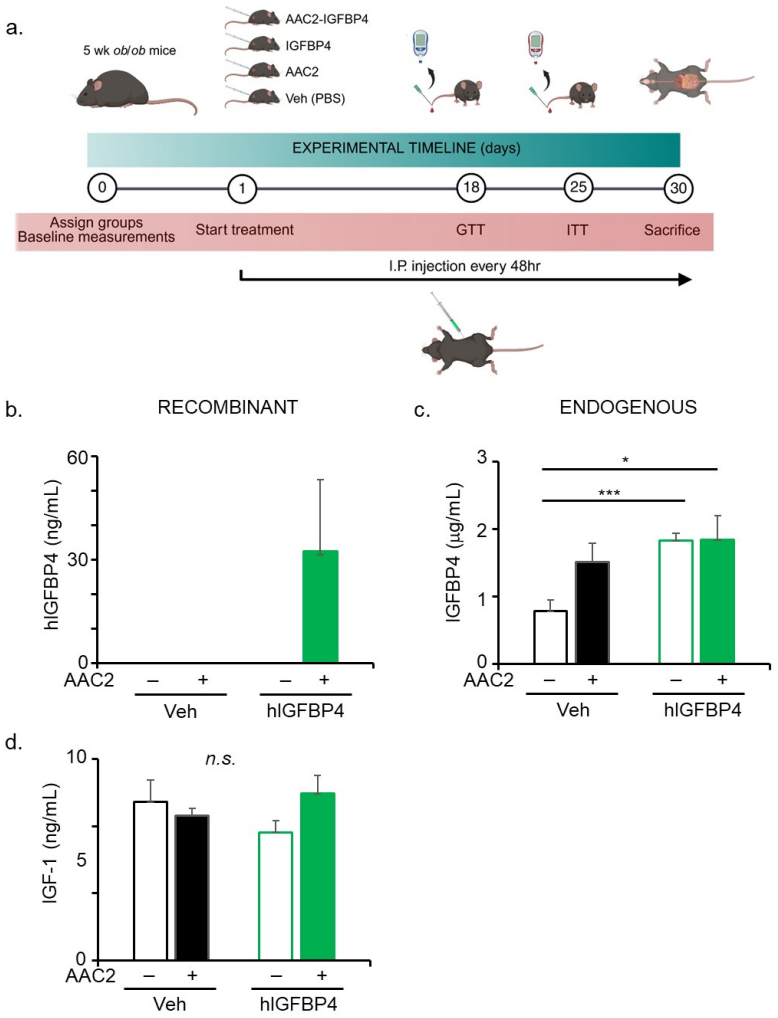

Fig. 3. AAC2-hIGFBP4 complex increased the circulation time of hIGFBP4 without influencing mouse IGFBP4 and IGF-1 levels. (a) schematic of the experiment showing four ob/ob male mouse groups (n = 5 per group) treated with control (veh, PBS), AAC2 (0.1 nmol/g body weight, BW), hIGFBP4 (1.79 nmol/g BW), or AAC2-hIGFBP4 (0.1 nmol/g and 1.79 nmol/g, respectively) every 48 h for 30 days. All data are shown and mean ± SEM. (b–d) plasma levels of

therapeutic hIGFBP4 (b), endogenous mouse IGFBP4 (c), and IGF1 (d) measured by ELISA 30 days after the start of treatment. n.s., not significant by unpaired Student's t-test.

therapeutic hIGFBP4 (b), endogenous mouse IGFBP4 (c), and IGF1 (d) measured by ELISA 30 days after the start of treatment. n.s., not significant by unpaired Student's t-test.

Food intake was also affected in *ob/ob* mice. Mice treated with AAC2 (–9%) or the AAC2-hIGFBP4 complex (–14%) showed significantly reduced food intake compared to the control group (**Fig. 4c**). Notably, mice receiving the AAC2-hIGFBP4 complex exhibited a progressive reduction in hyperphagia relative to other treated groups, despite having the highest baseline food intake among all groups (**Fig. 4d**). None of the treatments induced liver toxicity, as indicated by AST levels (**Fig. 4e**). However, a trend toward decreased liver weight ($P < 0.06$) was observed in *ob/ob* mice treated with the AAC2-hIGFBP4 complex. These findings demonstrate that AAC2-hIGFBP4 treatment leads to moderate but significant changes in the obesogenic and hyperphagic phenotype of *ob/ob* mice over the 30-day treatment period.

2.5 AAC2-hIGFBP4 complex, but not free hIGFBP4, markedly improved glucose metabolism in *ob/ob* mice

Untreated *ob/ob* mice developed severe insulin resistance (**Fig. 5a, b**) and glucose intolerance (**Fig. 5c, d**), as assessed by insulin

and glucose tolerance tests (ITT and GTT), respectively. Treatment with the AAC2-hIGFBP4 complex significantly improved insulin sensitivity in *ob/ob* mice, with enhanced ITT responses observed at 15 and 90 minutes following insulin injection compared to untreated *ob/ob* mice. A significant improvement at 90 minutes was also noted in the group treated with free hIGFBP4, while a trend toward improvement was seen in the AAC2-treated group (P= 0.085). GTT was performed 18 days after the start of treatment and revealed improved glucose tolerance in *ob/ob* mice treated with

399 the AAC2-hIGFBP4 complex at baseline, 15, 30, and 90 minutes after
400 glucose injection. In contrast, free hIGFBP4 and
401

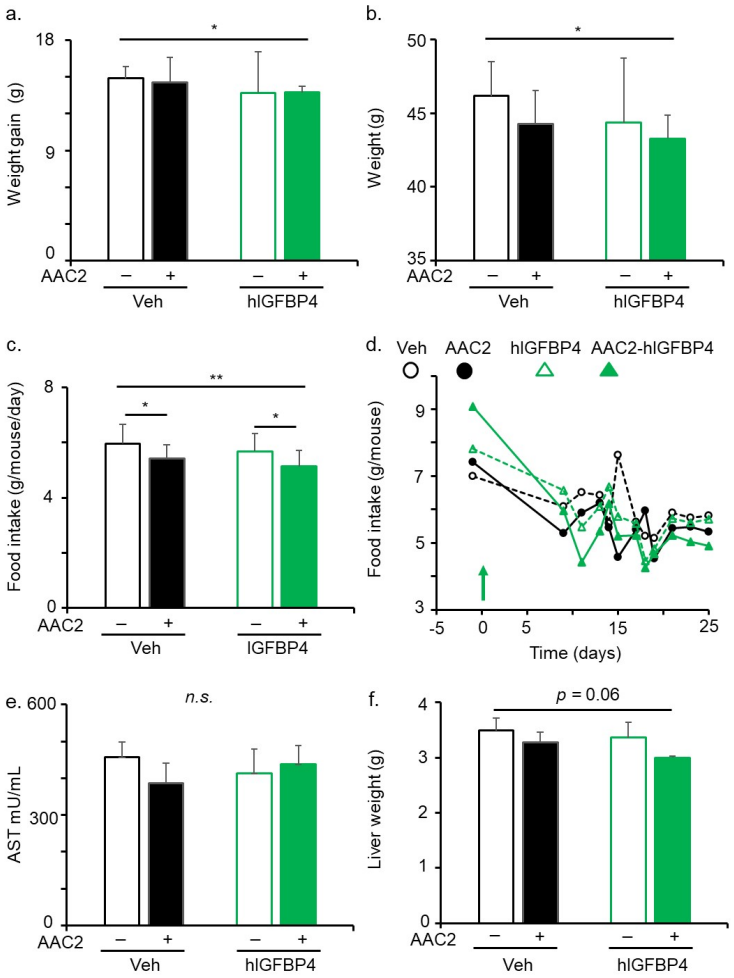

402 **Fig. 4. AAC2-hIGFBP4 complex induced moderate changes in weight**
403 **and food intake without causing liver toxicity in *ob/ob* mice.** (a, b)
404 weight gain after 30 days of treatment (a) and body weight at baseline (day
405 0) and at the end of the study (b) in the four groups of *ob/ob* mice described
406 in **Fig. 3.** (c, d) average food intake on day 25 (c) and food intake kinetics

over the course of the study in all *ob/ob* groups (d). (e) AST levels in plasma measured by ELISA at the end of the study. (f) liver weight in all mouse groups.

AAC2 treatments showed less pronounced effects. These effects were dependent on LepR, and treatment with the AAC2-hIGFBP4 complex, AAC2, or hIGFBP4, because the trend was reversed in *db/db* mice (**Fig. S1b**).

We also examined the contribution of insulin to glucose regulation in *ob/ob* mice. hIGFBP4 and AAC2 treatments had opposing effects on plasma insulin levels: AAC2 significantly increased insulin levels (169% of control), whereas hIGFBP4 reduced them (59.8% of control) (**Fig. 5e**). Paradoxically, treatment with the AAC2-hIGFBP4 complex also led to a decrease in circulating insulin levels (76% vs. 100% in controls), despite improved responses in both GTT and ITT. AAC2-induced hyperinsulinemia was absent in *db/db* mice, while treatment with hIGFBP4 and the AAC2-hIGFBP4 complex showed a similar trend toward reduced insulin levels (**Fig. S1c**) as observed in *ob/ob* mice (**Fig. 5e**).

The unique effect of the AAC2-hIGFBP4 complex was further demonstrated by the analysis of HbA1c levels. After just 30 days of treatment, HbA1c was markedly reduced (42.4% compared to 100% in controls) only in mice treated with the AAC2-hIGFBP4 complex (**Fig. 5f**). This is notable, given that 4–10 weeks are typically

431 required to observe changes in HbA1c in murine models of severe
432 insulin-dependent diabetes [43]. None of the other treatment groups
433 showed a trend toward HbA1c reduction, despite observed effects
434 on glucose regulation. Since AGEs are involved in the non-enzymatic
435 glycation of proteins, we also measured AGE levels in plasma (**Fig.**
436 **5g**)

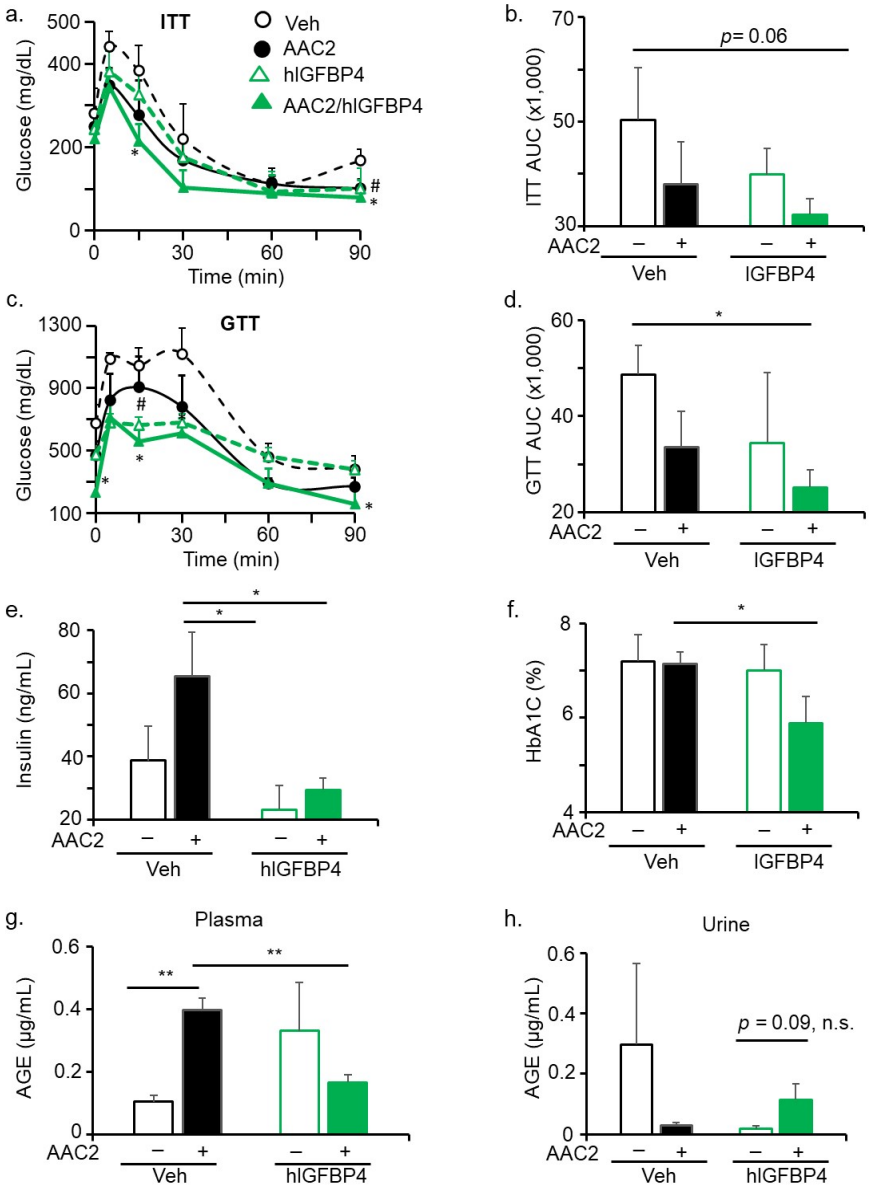

437 **Fig. 5. The AAC2-hIGFBP4 complex is more effective in improving**
438 **glucose regulation, reducing HbA1c, and modulating AGE handling**
439 **compared to individual components in *ob/ob* mice.** (a, b) kinetics of
440 blood glucose levels in 4-hour fasted *ob/ob* mice during ITT following a

single i.p. injection of human insulin (1 mU/g BW) (a) and corresponding area under the curve (AUC) analysis (b). (c, d) kinetics of blood glucose levels during GTT after a single i.p. injection of 10% glucose solution (10 µL/g BW) (c) and corresponding AUC analysis (d). (e) endogenous mouse insulin levels in plasma measured by ELISA at the end of the study (n = 5 per group). (f) HbA1c levels in blood measured by enzymatic colorimetric assay (n = 5 per group). (g, h) AGE levels measured in plasma (n = 5 per group) (g) and urine (n = 3 per group) (h) at the end of the study by enzymatic colorimetric assay. The reduced number of urine samples was due to spontaneous urination occurring before collection.

and urine (**Fig. 5h**) at the end of the study. Despite improved GTT responses, all treatment groups showed increased plasma AGE levels compared to controls (100%), with the highest elevation in the AAC2-treated group (377.7%), followed by the hIGFBP4 group (315.6%) and the AAC2-hIGFBP4 group (158.7%). These increases were statistically significant between the control and AAC2-treated groups. Notably, AGE levels in AAC2-hIGFBP4–treated mice were significantly lower than those in AAC2-treated *ob/ob* mice. Urinary AGE excretion was highest in the control group (100%) and lowest in the hIGFBP4 (6.3%) and AAC2 (9.8%) groups. A trend toward increased urinary AGE excretion was observed in the AAC2-hIGFBP4 group (38.7%) compared to free hIGFBP4. Together, these data highlight the unique metabolic profile of the AAC2-hIGFBP4

complex, which improved glucose uptake, reduced circulating insulin levels and HbA1c, without lowering AGE levels in plasma.

2.6 AAC2-hIGFBP4 complex induces expression of genes that support activation of the hepatic sinusoidal clearance system in *ob/ob* mice

To gain insight into the mechanisms underlying the responses to the AAC2-hIGFBP4 complex or its individual components, we performed transcriptome-wide gene expression analysis in the liver to identify genes distinguishing treatment effects in *ob/ob* mice. Strikingly, genes that changed significantly ($P < 0.005$) showed opposite regulatory patterns in response to free AAC2 versus the AAC2-hIGFBP4 complex (**Fig. 6a**). Based on these distinct expression profiles, we classified the genes into clusters I and II.

Treatments modulate TGFβ and hepatic sinusoidal clearance pathways.

The relationship among genes was assessed by pathway analysis, which highlighted the regulation of *Stab2* and *Fcgr1b* scavenger H receptors expressed by liver sinusoidal endothelial cells (LSEC) and serving as markers of LSEC [44] as central components of the cellular regulatory response (**Fig. 6b**, green line), downstream of TGFβ. Although changes in *Tgfb1* expression did not reach the significance threshold of $P < 0.005$, its expression differed significantly between livers from AAC2- and AAC2-hIGFBP4–treated

mice (**Fig. S2a**) and correlated with *Stab2* expression (**Fig. 6c**, R^2 = 0.52), as well as with other clearance receptors in cluster II, such as *Fcgr2b* (R^2 = 0.66) and *Mrc1* (R^2 = 0.65). These findings suggest that the expression of clearance scavenging machinery is associated with *Tgfb1* signaling. To further explore the signaling output of *Tgfb1*, we compared its expression with that of co-receptors *Tgfbr3* and *Eng*, as well as *Tgfbr2*, all of which showed significant correlations with *Tgfb1* (**Fig. 6d**).

The ALK5 (*Tgfbr1*) signaling pathway relies on the interaction of proteins encoded by *Tgfb1* with accessory *Tgfbr3*, *Tgfbr2*, and the obligate transcriptional co-activator *Smad4*. In our dataset, *Tgfb1* positively correlated with *Smad4* (**Fig. S2b**, R^2 = 0.36), which is known to regulate *Eng* expression [45]. Correspondingly, *Smad4* expression correlated with *Eng* (**Fig. S2c**, R^2 = 0.35).

Endoglin (Eng) is a central regulator of TGFβ network and cluster II gene expression in LSEC. In line with the pathway analysis placing *Eng* as a central component of the intracellular regulatory network (**Fig. 6b**), *Eng* expression correlated with 85% of all other genes in cluster II (**Fig. 6e**), including all LSEC-expressed scavenger receptors (**Fig. 6f**). Moreover, *Eng* expression was significantly correlated with *Kdr* encoding a critical *Eng*-dependent endothelial receptor VEGFR2 regulating vascular integrity [46] with other transmembrane proteins, including *Cdh5*

(VE-cadherin) and *Ptrpb* (**Fig. 6g**) [47]. *Eng* also correlated with *Pcxnc1*, a specific marker of LSEC, and *Pde2a*, a marker of differentiated LSEC [48, 49], suggesting that the majority of cluster II genes regulated by the AAC2-hIGFBP4 complex and AAC2 affect the function of the LSEC population (**Fig. 6e, g**).

Eng in LSEC mediates crosstalk with cluster I gene expression in other hepatic and sinusoidal cell populations. *Eng* also showed a strong correlation with *Ehd3*, which encodes a protein involved in trafficking of exosomes [50], as well as with secretory proteins such as *Igfbp1* and *Oit3* (**Fig. 6e**). Notably, *Oit3* is a bona fide selective marker for LSEC [51], along with *Dnase1l3* [52]. The expression of exosomal and secretory genes in LSEC suggests potential crosstalk with other hepatic cell types. In particular, *Ehd3* (R^2 = 0.70; **Fig. 6b**) and *Oit3* (R^2 = 0.35; **Fig. 7a**) exhibited significant correlations with the hepatic transcription factor *Klf9* [53]. Several hepatic genes, including *Dnajc15* [54] and *Gsta4* [55], are prominent in cluster I. These genes are inversely correlated with *Klf9* and show significant inter-correlation, including with *Nd6* (mitochondrial NADH dehydrogenase subunit 6), which is ubiquitously expressed [56]. An exception is *Scarna1*, which correlated only with *Dnajc15*, and *Slc51b* (also known as OSTβ), which is localized in cholangiocytes. *Slc51b* promotes the efflux of bile acids

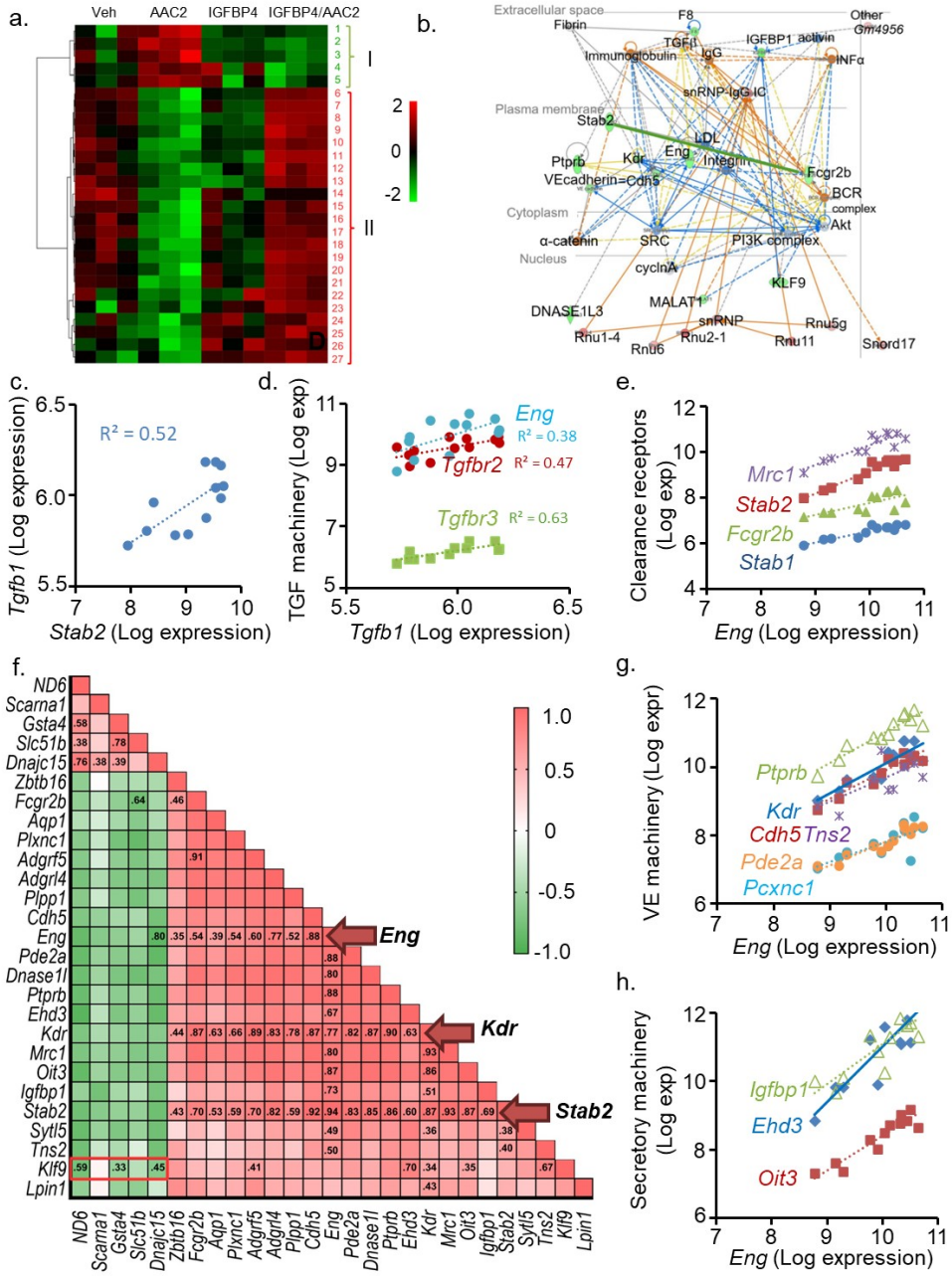

Fig. 6. Treatment with AAC2 and the AAC2-hIGFBP4 complex exhibits opposite patterns in the regulation of genes controlling liver sinusoidal clearance in *ob/ob* mice. (a) Heat map of gene expression in

livers from *ob/ob* mice treated with Veh, AAC2, hIGFBP4, or the AAC2-hIGFBP4 complex. Transcriptomic profiling was performed using Affymetrix microarrays, and genes with significant changes ($P < 0.005$) are shown. Cluster I includes: 1. *Dnajc15*, 2. *ND6*, 3. *Scarna1*, 4. *Slc51b*, 5. *Gsta4*. Cluster II includes: 6. *Mrc1*, 7. *Kdr*, 8. *Fcgr2b*, 9. *Adgrf5*, 10. *Adgrl4*, 11. *Plpp1*, 12. *Plxnc1*, 13. *Aqp1*, 14. *Igfbp1*, 15. *Cdh5*, 16. *Eng*, 17. *Stab2*, 18. *Pde2a*, 19. *Dnase1*, 20. *Ptprb*, 21. *Oit3*, 22. *Zbtb16*, 23. *Lpin1*, 24. *Sytl5*, 25. *Ehd3*, 26. *Tns2*, 27. *Klf9*. (b) Top-ranked pathway identified by Ingenuity Pathway Analysis, highlighting a TGFβ-driven regulatory network centered on the scavenger receptor axis involving *Stab2* and *Fcgr2b* (green line). (c–h) Pearson correlation analysis of gene expression across treated and untreated *ob/ob* mice. Gene expression values are shown in log scale; correlations with $R^2 > 0.33$ are considered significant ($P < 0.05$, n = 12). (c) Correlation between *Stab2* and *Tgfb1* expression. (d) Correlation between *Tgfb1* and its receptor and co-receptor genes (*Tgfbr2*, *Tgfbr3*, *Eng*), collectively referred to as TGFβ pathway machinery. (e) Correlation between *Eng* and LSEC clearance receptors, including *Stab1*, *Stab2* (scavenger receptor type H), *Mrc1* (mannose receptor C-type 1), and *Fcgr2b* (Fc receptor for clearance of immune complexes), collectively referred to as clearance receptors. (f) Heat map of correlation matrix analysis between all genes in clusters I and II with R^2 values. (g) Correlations between *Eng* and genes associated with vascular endothelium (VE) machinery: *Kdr*, *Cdh5*, *Ptprb*, *Tns2*, *Pde2a*, and *Pcxnc1*. (h) Correlations between *Eng* and genes encoding secretory proteins or proteins involved in exosomal trafficking, collectively referred to as secretory machinery.

and other compounds from hepatocytes into the sinusoidal blood [57] and is inversely regulated by the *Fcgr2b* clearance receptor. *Fcgr2b* also correlates with the transcription factor *Zbtb16* (**Fig. 6e**), a lineage marker for invariant natural killer T (iNKT) cells [58], which interacts with LSEC to support sinusoidal waste clearance [59, 60]. Additionally, *Fcgr2b* expression positively correlates with *Adgfr5* ($R^2 = 0.91$; Fig. 7c), a gene recently shown to regulate insulin clearance [61] in hepatic sinusoids and co-localized with endothelial cell marker in liver and other organs [62]. *Adgfr5* was upregulated by the AAC2-hIGFBP4 complex (**Fig. 2Sd**) and downregulated by AAC2 treatment compared to all other groups, consistent with reduced plasma insulin levels and a trend to improved insulin sensitivity. Taken together, these findings suggest that AAC2- and AAC2-hIGFBP4–regulated genes in LSEC also influence gene expression in other hepatic cell populations, including hepatocytes, cholangiocytes, and iNKT cells, that cooperate with the liver sinusoidal clearance system.

Eng expression is associated with genes in the ALK1 pathway underlying the fenestrated LSEC phenotype. The physiological angiocrine interaction between LSEC and other cell types, including hepatocytes and T cells [63], as well as the maintenance of LSEC fenestration and vascular integrity, requires dynamic switching

between the ALK5 and ALK1 pathways, which is regulated by endoglin (Alias:CD105, gene *Eng*) (**Box1**) [64-66].

Box 1. ALK5 and ALK1 TGFβ signaling in LSEC

The ALK5 pathway is mediated by **the classical TGFβ1 type I receptor**, TGFBR1 (gene: *Tgfbr1*). In this pathway, the TGFβ1 ligand is initially presented by the co-receptor TGFBR3 (*Tgfbr3*) to the type II receptor TGFBR2 (*Tgfbr2*), which then activates ALK5 and phosphorylates transcription factors SMAD2 and SMAD3 requiring co-SMAD, SMAD4 to regulate downstream gene expression, including *Eng*, *Kdr*, and *Cdh5*

Transition: Endoglin (*Eng*) interacts with TGFBR2 and TGFBR3, thereby attenuating ALK5 signaling and facilitating the shift toward alternative signaling pathways.

The ALK1 pathway is mediated by the alternative TGFβ type I receptor ACVRL1 (ALK1). Upon TGFβ1 binding, ALK1 activation results in phosphorylation of SMAD1 and SMAD5, which can signal with or without SMAD4. This pathway is predominant in endothelial cells and supports the maintenance of endothelial identity and fenestration in LSEC.

Transition: Endoglin also promotes endocytosis, favoring internalization and signaling via ALK1 over ALK5, thus reinforcing endothelial-specific TGFβ responses.

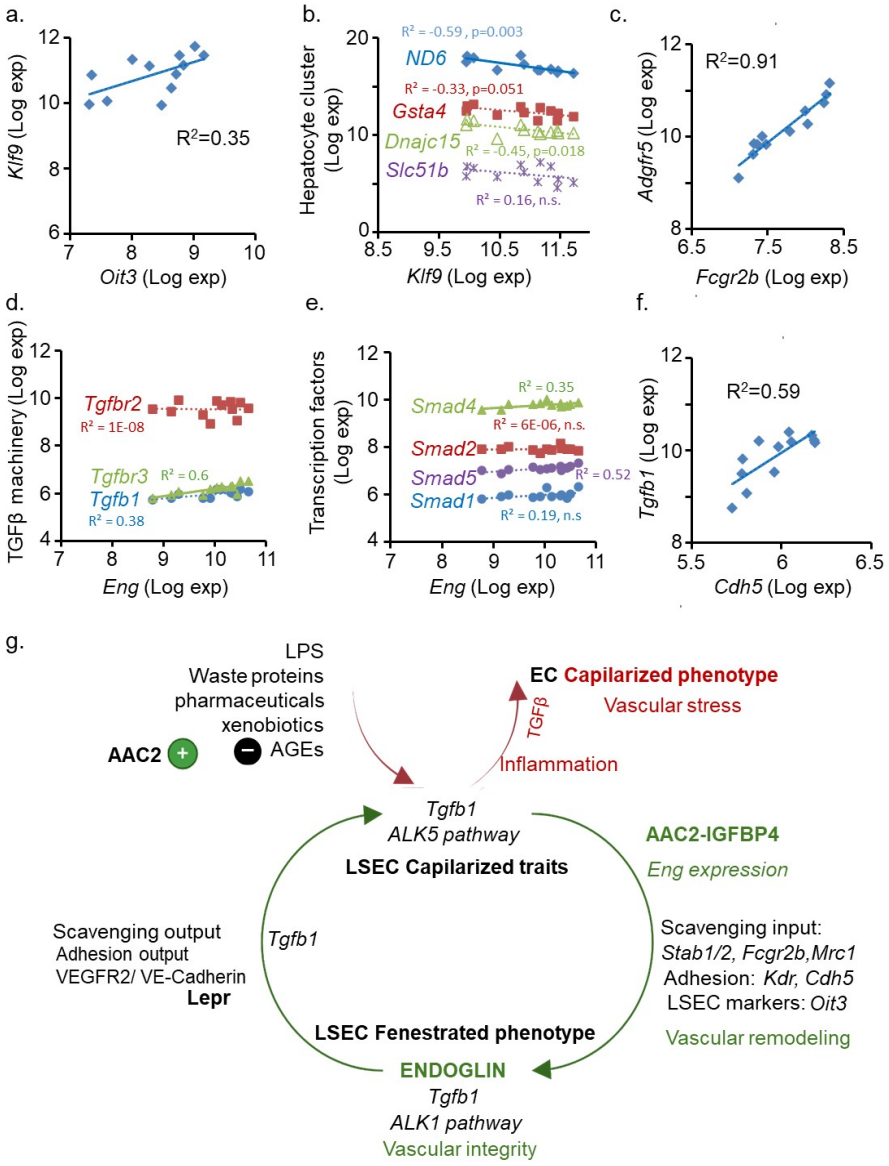

Fig. 7. Expression of Cluster II genes in LSECs and Cluster I genes in other hepatic cell populations supports the scavenging input hypothesis underlying AAC2 and AAC2-hIGFBP4 regulation of capillarized and fenestrated LSEC phenotypes. (a–g) Correlation and

mechanistic modeling support the scavenging input hypothesis underlying AAC2 and AAC2–hIGFBP4 regulation of LSEC phenotypes. (a–b) Cluster II genes expressed in LSECs significantly correlate with Cluster I genes expressed in other hepatic cell populations ($n = 12$, $R^2 > 0.33$, $P < 0.05$; Pearson correlation). Specifically, *Oit3* correlates positively with *Klf9* (a), while *Klf9* shows an inverse correlation with genes expressed in the hepatocyte-associated Cluster I (b). (c) *Eng* expression correlates with receptors of the TGFβ pathway and with *Tgfb1*. (d) *Fcgr2b* expression is positively correlated with *Adgrf5*. (e) *Eng* correlates with Smad family transcription factors. (f) *Cdh5* expression is positively associated with *Tgfb1*. (g) The proposed scavenging input hypothesis suggests that TGFβ production is stimulated by AGE uptake via stabilin 2 (*Stab2*), which activates the canonical ALK5 pathway underlying the capillarized LSEC phenotype and induces transcription of *Eng* and other Cluster II genes. Translation of *Eng* mRNA to protein endoglin defines the transition to ALK1 signaling, which, in conjunction with Cluster II proteins, promotes the fenestrated LSEC phenotype. Endoglin mediates endocytosis that terminates the ALK1 state. This physiological cycle is sustained by renewed scavenger activity, leptin receptor (*Lepr*), and VEGFR2/VE-cadherin signaling, which reinforce TGFβ production adapted for amount of waste in circulation. Binding of positively charged AGEs with AAC2 may reduce scavenger receptor input and suppress the fenestrated LSEC state, whereas the AAC2–hIGFBP4 complex promotes the transition toward a fenestrated phenotype. Inflammatory conditions disrupt this physiological TGFβ cycle in LSEC through cytokines (e.g., IL-11), accumulation of toxic waste, or TGFβ

derived from damaged or immune cells and drive a pathological process toward fibrosis.

Eng expression in our dataset correlated with *Tgfbr3* (R^2 = 0.60) and *Tgfb1* (R^2 = 0.38) (**Fig. 7c**), but not with *Tgfbr2*, which is agreement with its role in switching ALK5 to ALK1 pathways and subsequent endoglin-mediated ALK1 endocytosis [67]. Additionally, *Eng* expression correlated with *Smad5* and *Smad4* (**Fig. 7e**), transcription factors that mediate ALK1 signaling. Given that *Eng* is specifically expressed in LSEC in the liver [68], the ALK1/ALK5 regulatory switch is likely to occur in this cell population [64], mediating their fenestrated phenotype and signaling specificity.

Perpetuate TGFβ1 expression aligns with other LSEC genes targeted by AAC2-hIGFBP4 and its components. Strong correlations between *Tgfb1* and *Kdr* (R^2 = 0.61), as well as *Cdh5* (R^2 = 0.59), support the involvement of this pathway in maintaining constitutive *Tgfb1* expression in LSEC. These findings are consistent with previous reports that these genes and encoded VEGFR2/VE-Cadherin signaling cascade contribute to active TGFβ secretion characteristic for LSEC [66, 69]. Together, the increased expression of LSEC markers, clearance and scavenger H receptors, and transcriptional regulators in AAC2-hIGFBP4–treated *ob/ob* mice suggests the activation of the liver sinusoidal clearance system. In contrast, AAC2 alone appears to suppress the expression of genes

essential for sinusoidal clearance and the maintenance of the fenestrated LSEC phenotype.

3 Discussion

Our study demonstrates that binding with AAC2 nanofibers confers multiple advantageous properties to the natural scaffold protein IGFBP4, including increased circulation time and therapeutic improvements in weight gain, glucose tolerance, hyperinsulinemia, and insulin resistance in *ob/ob* mice. The most striking effect of the 30-day AAC2–IGFBP4 treatment was a reduction in HbA1c levels, lower than in any other group, coinciding with the upregulation of genes involved in liver sinusoidal clearance of AGE-modified compounds and other metabolic, environmental, pharmacological, and inflammatory waste products. In contrast, free AAC2 inhibited this clearance system, while free IGFBP4 had moderate, variable effects. Our study presents three main findings: 1) Apo-IGFBP4 regulates glucose uptake in vitro; 2) AAC2 serves as a therapeutic adjuvant enhancing glycemic control, and glycemic waste clearance in complex with IGFBP4; and 3) AAC2 and the AAC2–IGFBP4 complex act as opposing regulators of the LSEC-mediated sinusoidal clearance system, affecting clearance (*Mrc1* and *Fcgr2b*) and scavenger receptors (*Stab1/2*), and endoglin-dependent ALK5 and ALK1 pathways, (**Box1**) [64-66].

Current studies in genetically deficient *Igfbp4* mice [70] suggest that IGFBP4 interaction with IGF1 does not affect glucose tolerance or circulating IGF1 levels. Consistently, our pharmacological treatment with low concentrations of hIGFBP4 in *ob/ob* mice did not alter IGF1 levels and showed only a modest trend toward improved glucose tolerance. However, a moderate glucose uptake, promoting effect of apo-IGFBP4, was observed in vitro in human primary stromal vascular cells and murine fibroblasts. Upon binding with AAC2, apo-IGFBP4 acquired significant antidiabetic properties and formed a stable nanocomplex, distinguished by a characteristic ATR-FT-MIR spectral signature, AFM, and a shift in electrophoretic mobility due to its increased molecular weight. This interaction likely involves binding of IGFBP4's electronegative and hydrophobic regions to the positively charged, hydrophobic coumarin side chain of AAC2 [18]. Complex formation markedly increased the stability of hIGFBP4 in circulation, with detectable levels 48 hours post-injection, unlike free hIGFBP4, which was fully cleared within this timeframe. A similar stabilizing effect of AAC2 was previously reported for AAC2–insulin complexes [17]. Thus, AAC2 serves as a flexible nanoscaffold that can stabilize diverse therapeutic proteins.

The AAC2–hIGFBP4 complex appears to exhibit properties of both components, similar to what was observed with AAC2–insulin complexes [17]. AAC2 functions as an atypical activator of the leptin

receptor (LepR) [18], a central regulator of food intake, body weight, glucose tolerance, and insulin sensitivity [31]. Consistent with this, both free AAC2 and the AAC2-IGFBP4 complex led to reduced food intake and, to a lesser extent, weight gain. However, only treatment with the complex, where AAC2 acted additively with IGFBP4, resulted in a significant, robust, and less variable reduction in body weight, along with improved glucose tolerance, when compared to control *ob/ob* mice. In contrast, in *db/db* mice lacking LepR, the AAC2-hIGFBP4 complex failed to exert these beneficial effects on obesity and glucose metabolism. This highlights that AAC2-based protein complexes may acquire LepR-dependent properties, enabling them to overcome glucose tolerance.

Regulation of hyperinsulinemia in *ob/ob* mice revealed a dominant contribution of the hIGFBP4 component within the AAC2–hIGFBP4 complex. While AAC2 treatment alone tended to exacerbate hyperinsulinemia, an opposing trend was observed with hIGFBP4 alone, which reduced insulin levels. Notably, treatment with the AAC2–hIGFBP4 complex led to a significant reduction in circulating insulin, normalizing hyperinsulinemia in *ob/ob* mice. The AAC2-induced hyperinsulinemia was absent in *db/db* mice, indicating a LepR-dependent mechanism. Hyperinsulinemia is a well-documented feature of *ob/ob* mice and has been attributed to pancreatic β-cell hyperplasia [71], whereas in *db/db* mice, β-cell

number is not increased and progressively declines with age [72]. This divergence remains poorly understood and may reflect differences in LepR signaling or the presence of alternative LepR ligands [73]. In the context of the AAC2–hIGFBP4 complex, the observed reduction in hyperinsulinemia appeared to reflect IGFBP4 activity, independent of LepR status, in both *ob/ob* and *db/db* mice. These findings suggest that AAC2 and IGFBP4 may each retain distinct biological properties within the complex, acting through LepR-dependent (AAC2) or LepR-independent (IGFBP4) mechanisms. Remarkably, beyond exhibiting the characteristics of each component, the complex also regulated additional, unique pathways that prevented protein modifications under hyperglycemic conditions.

A striking effect of the AAC2–hIGFBP4 complex was the 19% lower HbA1c levels compared to both AAC2-treated and untreated hyperglycemic *ob/ob* mice after 30 days of treatment. Although mice have a shorter erythrocyte lifespan (40.7 ± 1.9 days; [74]) than humans (~120 days), such low HbA1c levels in *ob/ob* mice have previously been reported only with intensive antidiabetic therapies, such as high-dose metformin (150 mg/kg body weight; [75]), which exceeds typical human doses (14–30 mg/kg) by nearly tenfold. Notably, the HbA1c-lowering effect of the complex was dependent on LepR, as demonstrated in *db/db* mice, where HbA1c levels were

similar across all treated and untreated groups and indistinguishable from those observed in *ob/ob* mice treated with free AAC2 or hIGFBP4. These findings suggest that the AAC2–hIGFBP4 complex acquires novel properties that enable it to regulate specific, LepR-dependent metabolic pathways, which were revealed by liver transcriptomic analysis.

Transcriptomic analysis showed that all genes significantly altered ($p < 0.005$) fell into two categories: (1) defining the fenestrated liver sinusoidal clearance system, particularly LSEC (Cluster II) and (2) genes of other hepatic populations that correlate with LSEC genes (Cluster I). AAC2 and its complex modulated these gene sets in opposite directions while exhibiting a strong correlation, suggesting they act upon shared pathways but with opposing effects.

The liver sinusoidal clearance system is responsible for removing approximately 90% of circulating macromolecular waste, including circulating AGE [76], LPS [14, 77], lipoproteins, immune complexes [44], viruses [78], and nanomaterials [79]. Scavenging and endocytosis by fenestrated liver sinusoidal endothelial cells (LSEC) are central to coordinating responses with innate lymphoid (iNK) cells, cholangiocytes, hepatocytes, and Kupffer cells, thereby regulating immune and detoxification processes [79]. LSEC primarily recognize electronegative modifications of AGE-modified products through stabilin-1/stabilin-2 (*Stab1*/*Stab2*) and the

mannose receptor (Mrc1) [79], triggering regenerative, TGFβ-mediated physiological responses [80] and immunotolerance [81]. This clearance role contrasts with AGE recognition by the RAGE receptor and scavenger receptor type A in Kupffer cells and other immune populations, which activates inflammatory NFκB signaling [82]. In our study, the AAC2–hIGFBP4 complex robustly upregulated canonical fenestrated LSEC markers [51], along with genes associated with clearance and scavenger functions, while downregulating markers of iNK cells and cholangiocytes. In contrast, AAC2 alone exerted the opposite effect on these gene sets and was associated with the retention of AGEs in circulation. Importantly, neither AAC2 nor the AAC2–hIGFBP4 complex induced expression of inflammatory genes in vivo or in vitro. These findings support a model in which electrostatic interactions between positively charged AAC2 and negatively charged AGEs prevent both their LSEC-mediated clearance and engagement of RAGE-dependent inflammatory pathways. This is consistent with the unchanged HbA1c levels observed in AAC2-treated mice. However, as our current ELISA-based AGE measurements do not distinguish between free and AAC2-bound AGEs, further investigation is warranted to clarify the role of free AGE in modulating clearance activity and inflammation. Overall, the analysis of LSEC marker expression alongside other genes across treatment groups underscores the

dominant role of the liver sinusoidal clearance system in mediating the inhibitory effects of AAC2 and the activating effects of the AAC2–hIGFBP4 complex.

The mechanisms by which AAC2 and its complex regulate LSEC function were beyond the scope of this exploratory pilot study; however, our findings advance understanding of insufficiently characterized pathophysiology of LSECs. LSEC biology is defined by a dynamic transition between two distinct physiological stages. The capillarized phenotype is characterized by the expression of canonical endothelial markers and partial clearance function (**Fig. 7g**). Progression beyond this stage appears to depend on LepR signaling, as LepR-deficient *db/db* mice exhibit a predisposition to fibrosis [83]. In the mature stage, LSECs acquired a fenestrated morphology, robust clearance and endocytic capacities, and actively contribute to vascular regeneration and homeostasis. The mechanistic processes underlying this transition remain poorly understood and are subject to ongoing debate, despite the well-established involvement of TGFβ signaling in both stages [64, 84], which constitutes a limitation of this study.

TGFβ perpetuates a signaling cycle involving two principal pathways: ALK5 signaling in the capillarized state and ALK1 signaling in the fenestrated state [85]. This transition is mediated by

ALK5- and *Smad4*-dependent induction of *Eng* [86], which blocks ALK5 and promotes ALK1 signaling [64, 85]. This shift represents a pivotal change in transcriptional programming, as expression of *Eng*, *Kdr*, and scavenger receptors correlates with LSEC markers (*Oit3*, *Fcgr2b*, *Dnase1l3, Pde2a*, and *Pcxnc1* and others [44, 51]) in cluster 2 genes, suggesting a shared mechanism dependent on *Eng.* This TGFβ/ALK1/*Eng* interdependence was also evident and validated in genetic studies [85]. Indeed, endothelial-specific deletion of *Smad4* or *Eng* in mice results in severe vascular dysfunction and malformations [86, 87]. The translation of Eng mRNA into endoglin protein marks the shift toward an ALK1-dominant signaling phase, wherein ALK5 is suppressed [85]. This phase is terminated by endocytosis of endoglin–receptor complexes [67]. While the general framework of TGFβ signaling in LSECs is well described, our data suggest that its functional implementation depends on the scavenging process.

We propose a scavenger input model (**Fig. 7g**), supported by several lines of evidence: STAB2 role in clearance of AGE [88] and TGFβ [89], which regulate both ALK5 and ALK1 pathways in LSEC [64]. VEGFR2 and LepR signaling may also contribute to TGFβ production [66, 90]; development of fenestrated morphology has been demonstrated in response to VEGF [91]. Although STAB2 has been proposed to regulate TGFβ pathways and LSEC clearance

through interaction with its ligand TGFBi (TGFβ-induced) [92], TGFBi expression remained unchanged in this study, and AGE is likely a natural ligand for STAB2 under hyperglycemic conditions in *ob/ob* mice. Nevertheless, the development of both fibrosis and malfunction of TGFβ pathway in *Stab1/2*-deficient mice [92] underscores the essential role of scavenger input in promoting the fenestrated LSEC phenotype.

Given that STAB2 recognizes electronegative molecules such as AGEs, AAC2 may reduce scavenger H receptor engagement and atypically occupy LepR [18] and thereby prolong the capillarized phenotype of LSECs. Indeed, AAC2 treatment was associated with increased circulating AGE levels, reduced expression of *Eng* and its downstream targets, and unchanged HbA1c levels in *db/db* compared to *ob/ob* mice. Collectively, our findings support the hypothesis that AAC2 inhibits the transition to the fenestrated phenotype of LSECs. In contrast, the AAC2–IGFBP4 complex may mimic a modified form of the IGFBP4 scaffold with high affinity for STAB2 and/or other clearance receptors, thereby promoting *Eng* expression and facilitating LSEC fenestration. Further investigations are warranted to delineate the mechanisms underlying the inhibitory effects of AAC2 and the stimulatory effects of the AAC2–IGFBP4 complex. The specific action of AAC2 as an inhibitor and the AAC2–IGFBP4 complex as an activator of LSEC differentiation expands the

spectrum of therapeutic strategies, which currently focus on targeting the NO/RhoA/Rho-kinase pathway (e.g., statins), PPAR signaling, inflammatory cascades, and fibrinolytic mechanisms [93, 94]. Our study demonstrates that the AAC2–IGFBP4 complex has a distinct therapeutic profile: in addition to its glycemic benefits, it prevents HbA1c modification through mechanisms that improve LSEC functions.

The ability of AAC2 and its AAC2-IGFBP4 complex to modulate clearance properties at low concentrations holds promising potential for adjuvant applications. Transient inhibition of LSEC-mediated clearance by AAC2 may help reduce hepatic toxicity, environmental toxin exposure, or sepsis, particularly when combined with interventions such as blood transfusion. Temporally controlled, adjuvant use of LSEC clearance inhibitors may also enhance the efficacy of chemotherapeutic agents, vaccines, or gene therapy formulations that would otherwise be rapidly eliminated by the hepatic scavenging system. Conversely, activation of LSEC clearance could aid in reducing systemic waste accumulation associated with aging and various metabolic or degenerative diseases, approximately 45% of which are characterized by fibrosis.

4 Materials and Methods

4.1 Reagents

AAC2 compound ($C_{41}H_{50}N_6O_7$; $[M+H]^+$, ESI-MS 739.3819) was synthesized and characterized as previously described [18]. Human insulin (I9278, Sigma), human leptin (RP-8634, Invitrogen), and human IGFBP4 (350-05B, PeproTech) were obtained from commercial sources.

4.2 Human Subcutaneous Stromal Vascular Fraction (SVF) Preadipocytes

Informed consent and access to patients' medical records were obtained under protocols approved by the Institutional Review Board. Subcutaneous fat (SF) tissues were collected from overnight-fasted obese patients (see Supplementary Table S1) undergoing endoscopic hernia repair and/or bariatric procedures, including laparoscopic banding and gastric bypass surgeries. SVF cells were isolated from SF using Type I collagenase (Thermo Fisher Scientific, 17100017) and cultured in PGM-2 Preadipocyte Growth Medium-2 BulletKit (Lonza, PT-8002, supplemented with PT-9502; Basel, Switzerland) for 2–5 passages, as previously described [95].

4.3 Murine 3T3-L1 Fibroblast (Preadipocyte) Cultures

3T3-L1 preadipocytes (CL-173, ATCC) were maintained in high-glucose DMEM (Gibco, 11965) supplemented with 10% newborn calf serum (Gibco, 26010) and 1% Penicillin-Streptomycin (10,000 U/mL; Gibco, 15140). The medium was changed every 48 hours. Differentiation was induced using DMEM supplemented with 10% fetal bovine serum (FBS), 1.7 µM bovine insulin (Sigma, I0516), 1 µM dexamethasone (Sigma, D4902), and 0.5 mM 3-isobutyl-1-methylxanthine (IBMX; Sigma, I7018). After 48 hours, the medium was replaced with DMEM containing 10% FBS and 10 µg/mL insulin, and cells were maintained under these conditions for an additional 6 days, with medium changes every 48 hours.

4.4 IL-11 Reporter Cell Lines

HEK293 IL-11 reporter cells (Invivogen, hkb-hil11rv2) were cultured in T-150 flasks using complete growth medium consisting of high-glucose DMEM (Gibco) supplemented with 10% heat-inactivated fetal bovine serum (FBS; Gibco, A5268-01), 1% penicillin-streptomycin, and 5 mM L-glutamine. Upon reaching approximately 80% confluency, cells were trypsinized and seeded into 96-well plates (n = 4 per condition) in complete medium containing the following treatments: recombinant human IL-11 (rhIL-11, 1 ng/mL; R&D Systems, Cat# 218-IL-005), methylglyoxal (MGO, 10 µM; Sigma, Cat# M0252), AAC2 (1 µM), and human IGFBP4 (50 ng/mL;

PeproTech, Cat# 350-05B). Cells were incubated with treatments for 24 hours. IL-11 signaling activity was assessed using the Quanti-Blue assay (InvivoGen, Cat# rep-qbs) to detect secreted embryonic alkaline phosphatase (SEAP), which is produced in response to IL-11/STAT3 pathway activation. Absorbance was measured at 630 nm using a microplate reader. SEAP activity was normalized to total protein content, determined by a bicinchoninic acid (BCA) assay with absorbance read at 562 nm.

4.5 Glucose Uptake Assay

Cells were maintained in their standard high-glucose culture medium. Glucose uptake was assessed using the Cayman Chemical Glucose Uptake Assay Kit (Cat# 600470; Ann Arbor, MI) as previously described [18, 95]. Confluent cells cultured in 96-well plates were washed with Dulbecco's Phosphate-Buffered Saline (PBS; Sigma, D8537, St. Louis, MO) to remove residual glucose, followed by incubation with 200 µL/well of glucose-, phenol red-, and L-glutamine–free DMEM (Gibco, A14430; Waltham, MA). After incubation in starvation medium at 37°C for a defined period (see figure legends), the medium was replaced with DMEM containing 100 µg/mL of 2-deoxy-2-[(7-nitro-2,1,3-benzoxadiazol-4-yl)amino]-D-glucose (2-NBDG, FD-glucose), prepared from a 150 µg/mL working solution. Cells were incubated with FD-glucose at 37°C for 80 minutes. After incubation, cells were lysed, and fluorescence

intensity was measured at an excitation/emission of 485/535 nm using a Synergy H1 Hybrid Multi-Mode Microplate Reader (BioTek, Winooski, VT). Fluorescence values were normalized to total protein content per well.

4.6 Studies Examining Formation of the AAC2–hIGFBP4 Complex

4.6.1. Fourier Transform Infrared (FTIR) Spectroscopy. Molecular vibrations were analyzed for AAC2 (1 mM), recombinant human IGFBP4 (hIGFBP4, 10 ng/mL), a mixture of AAC2 (1 mM) with hIGFBP4 (10 ng/mL), and a mixture of AAC2 (1 mM) with heat-inactivated hIGFBP4 (10 ng/mL) in PBS. Heat inactivation of hIGFBP4 was performed by incubation at 90°C for 10 minutes to induce protein denaturation [96]. For FTIR measurements, 5 µL aliquots of each solution were placed on the attenuated total reflectance (ATR) crystal and vacuum-treated to remove solvent. A background spectrum was collected before each sample measurement. Spectra were acquired at a resolution of 8 cm^{-1} to improve the signal-to-noise ratio. All measurements (n = 3 per sample) were performed using an Agilent 4500 portable FTIR spectrometer (Agilent Technologies, Santa Clara, CA, USA) equipped with a 3-bounce diamond ATR crystal and a thermoelectrically cooled deuterated triglycine sulfate (DTGS)

detector. Data acquisition was performed using Agilent MicroLab PC software (Agilent Technologies Inc., Danbury, CT, USA).

4.6.2. Spectral Deconvolution Analysis. Changes in the secondary structure of human recombinant IGFBP4 protein and AAC2, which forms nanofibers under physiological pH [18], were analyzed using spectral deconvolution in the 1500–1700 cm^{-1} region [37]. Spectral data were processed in OriginPro 2024b (OriginLab, Northampton, MA, USA), including normalization and smoothing with a 5-point Savitzky–Golay filter, followed by a 7-point Savitzky–Golay second-derivative transformation. Spectral deconvolution was performed using the Multipeak fitting option with Gaussian band profile averaging, as described in [97]. Statistical analysis was conducted using one-way ANOVA with the Fisher test (OriginPro 2024b), and significance was set at $P < 0.05$.

4.6.3. Western Blot. The binding of AAC2 protein to hIGFBP4 and the denaturation of the complex were evaluated by native gel electrophoresis (Bio-Rad, Hercules, CA, USA). Each 10 µL sample was mixed with 5 µL of premixed native PAGE sample buffer (62.5 mM Tris-HCl, pH 6.8, 40% glycerol, 0.01% bromophenol blue). A total of 15 µL of each sample—hIGFBP4, heat-inactivated complex, and intact complex—was loaded onto 4–15% Mini-PROTEAN TGX™ Precast Protein Gels (Bio-Rad). Electrophoresis was performed using 1× Tris/Glycine buffer (25 mM Tris, 192 mM glycine, pH 8.3) for 2

hours at 90 V in an ice/water bath. A molecular weight marker (Precision Plus Protein™ Dual Color Standards, 10–250 kDa; Bio-Rad) was used as a reference.

4.6.4. Atomic Force Microscope (AFM).

AFM images were collected on the Bruker AXS Dimension Icon Atomic Force Microscope (Bruker AXS, Madison, WI) in ScanAsyst mode using Bruker AFM silicon tips with a nitride lever under a nitrogen atmosphere. 1mM AAC2 and 1mM AAC2 with 10ng/mL hIGFBP4 were prepared in PBS solution and allowed to incubate for 12 h. 20 µL of the samples were dropped on a freshly cleaved mica surface and dried before imaging with a resolution of 512 pixels × 512 pixels. AFM images were analyzed with Bruker NanoScope Analysis software.

4.7 Animal Studies

All animal procedures were approved by the Institutional Animal Care and Use Committee (IACUC) of The Ohio State University (OSU).

Five-week-old male leptin-deficient mice (homozygous for Lep^{ob}; stock number 000632) were purchased from The Jackson Laboratory (Bar Harbor, ME). Mice were maintained on a regular chow diet (Teklad LM-485 mouse/rat diet, irradiated; Envigo, Somerset, NJ) under a 12 h:12 h light–dark cycle. Following a one-week acclimation period, mice were randomly assigned to one

of four treatment groups: (1) Control group: received phosphate-buffered saline (PBS; 10 µL/g body weight [BW]); (2) AAC2 group: received AAC2 at 0.1 nmol/g BW; (3) hIGFBP4 group: received human IGFBP4 at 50 ng/g BW (equivalent to 1.79 nmol/g BW);AAC2-hIGFBP4 complex, contained hIGFBP4 (50 ng/g BW) and AAC2 (0.1 nmol/g BW). The components were mixed and allowed to stabilize complex at room temperature for 30 minutes prior to injection.

All treatments were administered in a total volume of 10 µL/g BW via subcutaneous injection into the scapular region every 48 hours for 4 weeks. Mice were not fasted prior to injections. Food intake and body weight were recorded weekly. At the study endpoint, mice were anesthetized via isoflurane inhalation, and blood was collected by cardiac puncture. EDTA-plasma and harvested organs were stored at –80 °C until analysis.

4.8 Glucose Tolerance Test (GTT) and Insulin Tolerance Test (ITT)

Three weeks after the initiation of treatment, glucose tolerance tests (GTT) were per-formed on mice fasted for 4 hours. Mice received an intraperitoneal (i.p.) injection of a 10% glucose solution at a dose of 10 µL/g body weight (BW). For insulin tolerance tests (ITT), mice were similarly fasted and injected i.p. with human insulin at 1 mU/g

BW. A recovery period of at least one week was allowed between the GTT and ITT procedures.

4.9 Biochemical Analysis

Plasma concentrations of human IGFBP4 (hIGFBP4; ab100542, Abcam), mouse IGFBP4 (RK02921, Abclonal), and mouse IGF1 (ab100695, Abcam) were measured by ELISA 30 days after the initiation of treatment. Aspartate aminotransferase (AST) activity was assessed in plasma using a commercial kit (ab105135, Abcam, Cambridge, UK). Human insulin levels in mouse plasma were quantified using ELISA (EZHI-14K, EMD Millipore, Billerica, MA), while mouse insulin was measured using a separate ELISA kit (EZRMI-13K, EMD Millipore). Hemoglobin A1c (HbA1c) levels in whole blood were determined using the Mouse HbA1c Assay Kit (#80310, Crystal Chem). Advanced glycation end products (AGEs) were measured in plasma and urine using an AGE ELISA kit (STA-817, Cell Biolabs). Total protein content in samples was normalized using the Pierce™ BCA Protein Assay Kit (23227, Thermo Fisher Scientific). Absorbance for all biochemical assays was measured using a Synergy H1 Hybrid Multi-Mode Microplate Reader (BioTek, Winooski, VT).

4.10 Affymetrix GeneChip Analysis

Total RNA was isolated using the RNeasy Kit (Qiagen, 74106, Hilden, Germany), and on-column DNA digestion was performed with the

RNase-Free DNase Set (Qiagen, 79254). RNA integrity was assessed using the Agilent 2100 BioAnalyzer (Agilent Technologies, Santa Clara, CA). A 100 ng aliquot of total RNA was linearly amplified, and 5.5 µg of resulting cDNA was labeled and fragmented using the GeneChip™ WT PLUS Reagent Kit (Affymetrix, 902280, Santa Clara, CA), following the manufacturer's protocol. Labeled cDNA targets were hybridized to Affymetrix GeneChip™ Mouse Gene ST 2.0 arrays for 16 h at 45 °C with rotation at 60 rpm. Arrays were washed and stained using the Fluidics Station 450 (Thermo Fisher, 00-0079, Waltham, MA) and scanned with the GeneChip™ Scanner 3000 (Thermo Fisher, 00-0210).

Signal intensities were quantified using the Affymetrix Expression Console software, version 1.3.1 (Thermo Fisher). Background correction and quantile normalization were applied to reduce technical variation, and probe-set expression values were calculated using the Robust Multi-array Average (RMA) method. After applying a noise cutoff filter, 9,528 probe sets were retained for statistical analysis. A linear modeling approach was used, incorporating a variance smoothing method and fully moderated t-statistics. Multiple testing correction was applied to control the expected number of false positives.

4.11 Statistical Analysis

All data are presented as mean ± SEM. The number of biological replicates for each assay is indicated in the corresponding figure legends. Group comparisons were performed using an unpaired Student's *t*-test or one-way ANOVA, as appropriate. A P value < 0.05 was considered statistically significant and is indicated by an asterisk. For gene expression analysis, a more stringent significance threshold of $P < 0.005$ was applied to control for the expected 5 false positives per 1000 tests. Correlation heatmaps were generated using GraphPad Prism, and the coefficient of determination (R^2) was calculated using R programming. Pearson correlation was used for gene expression comparisons ($n = 12$); correlations with $R^2 > 0.33$ were considered statistically significant ($p < 0.05$). Ingenuity Pathways Analysis (IPA) software was used for pathway analysis.

5 Conclusions

The current study, along with previous work, suggests that AAC2 possesses the properties of a therapeutic modular platform that can be used alone or in combination with established (e.g., insulin) and novel (e.g., IGFBP4) proteins to adapt and optimize their efficacy across diverse and multifunctional therapeutic applications. Specifically, the AAC2-IGFBP4 complex improves hyperglycemia, hyperinsulinemia, as well as HbA1C via induction of LSECs and their

clearance genes. Activation of LSEC clearance aid in reducing systemic waste accumulation associated with aging [98], and various metabolic or degenerative diseases, approximately 45% of which are characterized by fibrosis.

The ability of AAC2 and its complex to modulate clearance properties at low concentrations holds considerable promise as adjuvant agents in pharmacological or nanotherapeutic strategies, particularly, given that approximately 90 % of blood-borne adenoviruses or virus-like nanoparticles are cleared by LSECs [79]. Furthermore, temporally controlled use of LSEC clearance inhibitors could enhance the efficacy of chemotherapeutic agents, vaccines, or gene therapy formulations by delaying their rapid LSEC-mediated hepatic elimination.

Funding: This research was funded by the National Science Foundation (CHE-2106924) (J.R.P.) and by the Ralph and Marian Falk Medical Research Catalyst Award (J.R.P. and O.Z); National Institute of Allergy and Infectious Diseases (NIAID) grant AI170880 (L.P.G).

Availability of data and materials: All data generated or analyzed during this study are included in this published article and its supplementary information files. The full Affymetrix datasets used

and/or analyzed during the current study are available from the corresponding author on reasonable request.

References

1. Collaborators, G.B.D.D.: Global, regional, and national burden of diabetes from 1990 to 2021, with projections of prevalence to 2050: a systematic analysis for the Global Burden of Disease Study 2021. Lancet 402 (10397), 203–234 (2023).
2. Patel, S.A.: Diabetes Complications in the U.S.: Following the Data to Guide Comprehensive Action. Diabetes Care 48 (1), 15–17 (2025).
3. Kato, S., Matsumura T., Sugawa H., et al.: Correlation between serum advanced glycation end-products and vascular complications in patient with type 2 diabetes. Sci Rep 14 (1), 18722 (2024).
4. Katsiki, N., Kolovou G., Melidonis A., et al.: The Cardiac-Kidney-Liver (CKL) syndrome: the "real entity" of type 2 diabetes mellitus. Arch Med Sci 20 (1), 207–215 (2024).
5. Tuleta, I., Frangogiannis N.G.: Diabetic fibrosis. Biochim Biophys Acta Mol Basis Dis 1867 (4), 166044 (2021).
6. Calcutt, N.A., Cooper M.E., Kern T.S., et al.: Therapies for hyperglycaemia-induced diabetic complications: from animal models to clinical trials. Nat Rev Drug Discov 8 (5), 417–429 (2009).
7. Schalkwijk, C.G., Micali L.R., Wouters K.: Advanced glycation endproducts in diabetes-related macrovascular complications: focus on methylglyoxal. Trends Endocrinol Metab 34 (1), 49–60 (2023).
8. Oliveira, A.L., de Oliveira M.G., Monica F.Z., et al.: Methylglyoxal and Advanced Glycation End Products (AGEs): Targets for the Prevention and Treatment of Diabetes-Associated Bladder Dysfunction? Biomedicines 12 (5), (2024).
9. Xue, L., Zhang Y., Zhang Q.: The relationship between advanced glycation end products, metabolic metrics, HbA(1c,) and diabetic nephropathy. Front Endocrinol (Lausanne) 16 1468737 (2025).
10. Khalid, M., Petroianu G., Adem A.: Advanced Glycation End Products and Diabetes Mellitus: Mechanisms and Perspectives. Biomolecules 12 (4), (2022).
11. Elshoff, D., Mehta P., Ziouzenkova O.: Chronic Kidney Disease Diets for Kidney Failure Prevention: Insights from the IL-11 Paradigm. Nutrients 16 (9), (2024).
12. Politz, O., Gratchev A., McCourt P.A., et al.: Stabilin-1 and -2 constitute a novel family of fasciclin-like hyaluronan receptor homologues. Biochem J 362 (Pt 1), 155–164 (2002).

13. Hansen, B., Longati P., Elvevold K., et al.: Stabilin-1 and stabilin-2 are both directed into the early endocytic pathway in hepatic sinusoidal endothelium via interactions with clathrin/AP-2, independent of ligand binding. Exp Cell Res 303 (1), 160–173 (2005).
14. Cabral, F., Al-Rahem M., Skaggs J., et al.: Stabilin receptors clear LPS and control systemic inflammation. iScience 24 (11), 103337 (2021).
15. Schledzewski, K., Geraud C., Arnold B., et al.: Deficiency of liver sinusoidal scavenger receptors stabilin-1 and -2 in mice causes glomerulofibrotic nephropathy via impaired hepatic clearance of noxious blood factors. J Clin Invest 121 (2), 703–714 (2011).
16. Tsuchiya, K., Accili D.: Liver sinusoidal endothelial cells link hyperinsulinemia to hepatic insulin resistance. Diabetes 62 (5), 1478–1489 (2013).
17. Lee, A., Mason M.L., Lin T., et al.: Amino Acid Nanofibers Improve Glycemia and Confer Cognitive Therapeutic Efficacy to Bound Insulin. Pharmaceutics 14 (1), (2021).
18. Lee, A., Sun Y., Lin T., et al.: Amino acid-based compound activates atypical PKC and leptin receptor pathways to improve glycemia and anxiety like behavior in diabetic mice. Biomaterials 239 119839 (2020).
19. Ma, L.Z., Liu W.S., He Y., et al.: Plasma proteomics identify novel biomarkers and dynamic patterns of biological aging. J Adv Res (2025).
20. Forbes, B.E., McCarthy P., Norton R.S.: Insulin-like growth factor binding proteins: a structural perspective. Front Endocrinol (Lausanne) 3 38 (2012).
21. Zhu, W., Shiojima I., Ito Y., et al.: IGFBP-4 is an inhibitor of canonical Wnt signalling required for cardiogenesis. Nature 454 (7202), 345–349 (2008).
22. Maridas, D.E., DeMambro V.E., Le P.T., et al.: IGFBP4 Is Required for Adipogenesis and Influences the Distribution of Adipose Depots. Endocrinology 158 (10), 3488–3500 (2017).
23. Yang, K., Adin C., Shen Q., et al.: Aldehyde dehydrogenase 1 a1 regulates energy metabolism in adipocytes from different species. Xenotransplantation 24 (5), (2017).
24. Ziouzenkova, O., Orasanu G., Sharlach M., et al.: Retinaldehyde represses adipogenesis and diet-induced obesity. Nat Med 13 (6), 695–702 (2007).
25. Lewitt, M.S., Dent M.S., Hall K.: The Insulin-Like Growth Factor System in Obesity, Insulin Resistance and Type 2 Diabetes Mellitus. J Clin Med 3 (4), 1561–1574 (2014).
26. Laursen, L.S., Kjaer-Sorensen K., Andersen M.H., et al.: Regulation of insulin-like growth factor (IGF) bioactivity by sequential proteolytic cleavage of IGF binding protein-4 and -5. Mol Endocrinol 21 (5), 1246–1257 (2007).

27. Milman, S., Atzmon G., Huffman D.M., et al.: Low insulin-like growth factor-1 level predicts survival in humans with exceptional longevity. Aging Cell 13 (4), 769–771 (2014).
28. Hoeflich, A., David R., Hjortebjerg R.: Current IGFBP-Related Biomarker Research in Cardiovascular Disease-We Need More Structural and Functional Information in Clinical Studies. Front Endocrinol (Lausanne) 9 388 (2018).
29. Wo, D., Peng J., Ren D.N., et al.: Opposing Roles of Wnt Inhibitors IGFBP-4 and Dkk1 in Cardiac Ischemia by Differential Targeting of LRP5/6 and beta-catenin. Circulation 134 (24), 1991–2007 (2016).
30. Singh, R., De Aguiar R.B., Naik S., et al.: LRP6 enhances glucose metabolism by promoting TCF7L2-dependent insulin receptor expression and IGF receptor stabilization in humans. Cell Metab 17 (2), 197–209 (2013).
31. Friedman, J.: The long road to leptin. J Clin Invest 126 (12), 4727–4734 (2016).
32. Sitar, T., Popowicz G.M., Siwanowicz I., et al.: Structural basis for the inhibition of insulin-like growth factors by insulin-like growth factor-binding proteins. Proc Natl Acad Sci U S A 103 (35), 13028–13033 (2006).
33. Widjaja, A.A., Viswanathan S., Shekeran S.G., et al.: Targeting endogenous kidney regeneration using anti-IL11 therapy in acute and chronic models of kidney disease. Nat Commun 13 (1), 7497 (2022).
34. Vangrieken, P., Scheijen J., Schiffers P.M.H., et al.: Modelling the effects of elevated methylglyoxal levels on vascular and metabolic complications. Sci Rep 15 (1), 6025 (2025).
35. Schalkwijk, C.G., Stehouwer C.D.A.: Methylglyoxal, a Highly Reactive Dicarbonyl Compound, in Diabetes, Its Vascular Complications, and Other Age-Related Diseases. Physiol Rev 100 (1), 407–461 (2020).
36. Gkinali, A.A., Matsakidou A., Paraskevopoulou A.: Characterization of Tenebrio molitor Larvae Protein Preparations Obtained by Different Extraction Approaches. Foods 11 (23), (2022).
37. Yang, H., Yang S., Kong J., et al.: Obtaining information about protein secondary structures in aqueous solution using Fourier transform IR spectroscopy. Nat Protoc 10 (3), 382–396 (2015).
38. Chen, W., Zhu J., Wang W., et al.: Characterization of whey protein isolate-(-)-epigallocatechin-3-gallate conjugates prepared by non-enzymatic and enzymatic methods and their application in stabilizing beta-carotene emulsion. Food Chem 399 133727 (2023).
39. Murciano-Calles, J., Marin-Argany M., Cobos E.S., et al.: The impact of extra-domain structures and post-translational modifications in the folding/misfolding behaviour of the third PDZ domain of MAGUK neuronal protein PSD-95. PLoS One 9 (5), e98124 (2014).
40. Grewal, M.K., Huppertz T., Vasiljevic T.: FTIR fingerprinting of structural changes of milk proteins induced by heat treatment, deamidation and dephosphorylation. Food Hydrocolloid 80 160–167 (2018).

41. Ivanov, Y.D., Pleshakova T.O., Shumov I.D., et al.: AFM Imaging of Protein Aggregation in Studying the Impact of Knotted Electromagnetic Field on A Peroxidase. Sci Rep 10 (1), 9022 (2020).
42. Haywood, N.J., Slater T.A., Matthews C.J., et al.: The insulin like growth factor and binding protein family: Novel therapeutic targets in obesity & diabetes. Mol Metab 19 86–96 (2019).
43. Dan, K., Fujita H., Seto Y., et al.: Relation between stable glycated hemoglobin A1C and plasma glucose levels in diabetes-model mice. Exp Anim 46 (2), 135–140 (1997).
44. Ganesan, L.P., Kim J., Wu Y., et al.: FcgammaRIIb on liver sinusoidal endothelium clears small immune complexes. J Immunol 189 (10), 4981–4988 (2012).
45. Ola, R., Kunzel S.H., Zhang F., et al.: SMAD4 Prevents Flow Induced Arteriovenous Malformations by Inhibiting Casein Kinase 2. Circulation 138 (21), 2379–2394 (2018).
46. Zhang, Q., Wang C., Cannavicci A., et al.: Endoglin deficiency impairs VEGFR2 but not FGFR1 or TIE2 activation and alters VEGF-mediated cellular responses in human primary endothelial cells. Transl Res 235 129–143 (2021).
47. de Haan, W., Oie C., Benkheil M., et al.: Unraveling the transcriptional determinants of liver sinusoidal endothelial cell specialization. Am J Physiol Gastrointest Liver Physiol 318 (4), G803–G815 (2020).
48. Halpern, K.B., Shenhav R., Massalha H., et al.: Paired-cell sequencing enables spatial gene expression mapping of liver endothelial cells. Nat Biotechnol 36 (10), 962–970 (2018).
49. Tabula Muris, C., Overall c., Logistical c., et al.: Single-cell transcriptomics of 20 mouse organs creates a Tabula Muris. Nature 562 (7727), 367–372 (2018).
50. Naslavsky, N., Rahajeng J., Sharma M., et al.: Interactions between EHD proteins and Rab11-FIP2: a role for EHD3 in early endosomal transport. Mol Biol Cell 17 (1), 163–177 (2006).
51. Li, Z.W., Ruan B., Yang P.J., et al.: Oit3, a promising hallmark gene for targeting liver sinusoidal endothelial cells. Signal Transduct Target Ther 8 (1), 344 (2023).
52. Kalucka, J., de Rooij L., Goveia J., et al.: Single-Cell Transcriptome Atlas of Murine Endothelial Cells. Cell 180 (4), 764–779 e720 (2020).
53. Cui, A., Fan H., Zhang Y., et al.: Dexamethasone-induced Kruppel-like factor 9 expression promotes hepatic gluconeogenesis and hyperglycemia. J Clin Invest 129 (6), 2266–2278 (2019).
54. Iruzubieta, P., Goikoetxea-Usandizaga N., Barbier-Torres L., et al.: Boosting mitochondria activity by silencing MCJ overcomes cholestasis-induced liver injury. JHEP Rep 3 (3), 100276 (2021).
55. Shimizu, T., Fan Y., Yamana D., et al.: Glutathione S-transferase A4 is a positive marker for rat hepatic foci induced by clofibrate and genotoxic carcinogens. Cancer Sci 101 (5), 1093–1098 (2010).

56. Pirola, C.J., Gianotti T.F., Burgueno A.L., et al.: Epigenetic modification of liver mitochondrial DNA is associated with histological severity of nonalcoholic fatty liver disease. Gut 62 (9), 1356–1363 (2013).
57. Beaudoin, J.J., Bezencon J., Sjostedt N., et al.: Role of Organic Solute Transporter Alpha/Beta in Hepatotoxic Bile Acid Transport and Drug Interactions. Toxicol Sci 176 (1), 34–35 (2020).
58. Park, J.Y., DiPalma D.T., Kwon J., et al.: Quantitative Difference in PLZF Protein Expression Determines iNKT Lineage Fate and Controls Innate CD8 T Cell Generation. Cell Rep 27 (9), 2548–2557 e2544 (2019).
59. Papaioannou, S., See J.X., Jeong M., et al.: Liver sinusoidal endothelial cells orchestrate NK cell recruitment and activation in acute inflammatory liver injury. Cell Rep 42 (8), 112836 (2023).
60. Wohlleber, D., Knolle P.A.: The role of liver sinusoidal cells in local hepatic immune surveillance. Clin Transl Immunology 5 (12), e117 (2016).
61. Rothe, J., Kraft R., Ricken A., et al.: The adhesion GPCR GPR116/ADGRF5 has a dual function in pancreatic islets regulating somatostatin release and islet development. Commun Biol 7 (1), 104 (2024).
62. Lu, S., Liu S., Wietelmann A., et al.: Developmental vascular remodeling defects and postnatal kidney failure in mice lacking Gpr116 (Adgrf5) and Eltd1 (Adgrl4). PLoS One 12 (8), e0183166 (2017).
63. Gao, J., Lan T., Kostallari E., et al.: Angiocrine signaling in sinusoidal homeostasis and liver diseases. J Hepatol 81 (3), 543–561 (2024).
64. Lebrin, F., Goumans M.J., Jonker L., et al.: Endoglin promotes endothelial cell proliferation and TGF-beta/ALK1 signal transduction. EMBO J 23 (20), 4018–4028 (2004).
65. Guo, B., Slevin M., Li C., et al.: CD105 inhibits transforming growth factor-beta-Smad3 signalling. Anticancer Res 24 (3a), 1337–1345 (2004).
66. Rudini, N., Felici A., Giampietro C., et al.: VE-cadherin is a critical endothelial regulator of TGF-beta signalling. EMBO J 27 (7), 993–1004 (2008).
67. Tazat, K., Pomeraniec-Abudy L., Hector-Greene M., et al.: ALK1 regulates the internalization of endoglin and the type III TGF-beta receptor. Mol Biol Cell 32 (7), 605–621 (2021).
68. Eissazadeh, S., Mohammadi S., Faradonbeh F.A., et al.: Endoglin and soluble endoglin in liver sinusoidal endothelial dysfunction in vivo. Biochim Biophys Acta Mol Basis Dis 1870 (3), 166990 (2024).
69. Braczkowski, M.J., Kufel K.M., Kulinska J., et al.: Pleiotropic Action of TGF-Beta in Physiological and Pathological Liver Conditions. Biomedicines 12 (4), (2024).
70. Ning, Y., Schuller A.G., Bradshaw S., et al.: Diminished growth and enhanced glucose metabolism in triple knockout mice containing mutations of insulin-like growth factor binding protein-3, -4, and -5. Mol Endocrinol 20 (9), 2173–2186 (2006).
71. Tomita, T., Doull V., Pollock H.G., et al.: Pancreatic islets of obese hyperglycemic mice (ob/ob). Pancreas 7 (3), 367–375 (1992).

72. Dalboge, L.S., Almholt D.L., Neerup T.S., et al.: Characterisation of age-dependent beta cell dynamics in the male db/db mice. PLoS One 8 (12), e82813 (2013).
73. Song, N.J., Lee A., Yasmeen R., et al.: Epiregulin as an Alternative Ligand for Leptin Receptor Alleviates Glucose Intolerance without Change in Obesity. Cells 11 (3), (2022).
74. Van Putten, L.M.: The life span of red cells in the rat and the mouse as determined by labeling with DFP32 in vivo. Blood 13 (8), 789–794 (1958).
75. Yoo, J., Park J.E., Han J.S.: HMC Ameliorates Hyperglycemia via Acting PI3K/AKT Pathway and Improving FOXO1 Pathway in ob/ob Mice. Nutrients 15 (9), (2023).
76. Smedsrod, B., Melkko J., Araki N., et al.: Advanced glycation end products are eliminated by scavenger-receptor-mediated endocytosis in hepatic sinusoidal Kupffer and endothelial cells. Biochem J 322 (Pt 2) (Pt 2), 567–573 (1997).
77. Yao, Z., Mates J.M., Cheplowitz A.M., et al.: Blood-Borne Lipopolysaccharide Is Rapidly Eliminated by Liver Sinusoidal Endothelial Cells via High-Density Lipoprotein. J Immunol 197 (6), 2390–2399 (2016).
78. Ganesan, L.P., Mohanty S., Kim J., et al.: Rapid and efficient clearance of blood-borne virus by liver sinusoidal endothelium. PLoS Pathog 7 (9), e1002281 (2011).
79. Bhandari, S., Larsen A.K., McCourt P., et al.: The Scavenger Function of Liver Sinusoidal Endothelial Cells in Health and Disease. Front Physiol 12 757469 (2021).
80. Olsavszky, V., Sticht C., Schmid C.D., et al.: Exploring the transcriptomic network of multi-ligand scavenger receptor Stabilin-1- and Stabilin-2-deficient liver sinusoidal endothelial cells. Gene 768 145284 (2021).
81. Carambia, A., Freund B., Schwinge D., et al.: TGF-beta-dependent induction of CD4(+)CD25(+)Foxp3(+) Tregs by liver sinusoidal endothelial cells. J Hepatol 61 (3), 594–599 (2014).
82. Xue, J., Rai V., Singer D., et al.: Advanced glycation end product recognition by the receptor for AGEs. Structure 19 (5), 722–732 (2011).
83. Trak-Smayra, V., Paradis V., Massart J., et al.: Pathology of the liver in obese and diabetic ob/ob and db/db mice fed a standard or high-calorie diet. Int J Exp Pathol 92 (6), 413–421 (2011).
84. Goumans, M.J., Valdimarsdottir G., Itoh S., et al.: Balancing the activation state of the endothelium via two distinct TGF-beta type I receptors. EMBO J 21 (7), 1743–1753 (2002).
85. Oh, S.P., Seki T., Goss K.A., et al.: Activin receptor-like kinase 1 modulates transforming growth factor-beta 1 signaling in the regulation of angiogenesis. Proc Natl Acad Sci U S A 97 (6), 2626–2631 (2000).
86. Crist, A.M., Lee A.R., Patel N.R., et al.: Vascular deficiency of Smad4 causes arteriovenous malformations: a mouse model of Hereditary Hemorrhagic Telangiectasia. Angiogenesis 21 (2), 363–380 (2018).

87. Li, D.Y., Sorensen L.K., Brooke B.S., et al.: Defective angiogenesis in mice lacking endoglin. Science 284 (5419), 1534–1537 (1999).
88. Tamura, Y., Adachi H., Osuga J., et al.: FEEL-1 and FEEL-2 are endocytic receptors for advanced glycation end products. J Biol Chem 278 (15), 12613–12617 (2003).
89. He, W., Zhang J., Gan T.Y., et al.: Advanced glycation end products induce endothelial-to-mesenchymal transition via downregulating Sirt 1 and upregulating TGF-beta in human endothelial cells. Biomed Res Int 2015 684242 (2015).
90. Wolf, G., Hamann A., Han D.C., et al.: Leptin stimulates proliferation and TGF-beta expression in renal glomerular endothelial cells: potential role in glomerulosclerosis [seecomments]. Kidney Int 56 (3), 860–872 (1999).
91. Tian, S.P., Ge J.Y., Song Y.M., et al.: A novel efficient strategy to generate liver sinusoidal endothelial cells from human pluripotent stem cells. Sci Rep 14 (1), 13831 (2024).
92. Krzistetzko, J., Geraud C., Dormann C., et al.: Association of Differentially Altered Liver Fibrosis with Deposition of TGFBi in Stabilin-Deficient Mice. Int J Mol Sci 24 (13), (2023).
93. Gao, J., Zuo B., He Y.: Liver sinusoidal endothelial cells as potential drivers of liver fibrosis (Review). Mol Med Rep 29 (3), (2024).
94. McConnell, M.J., Kostallari E., Ibrahim S.H., et al.: The evolving role of liver sinusoidal endothelial cells in liver health and disease. Hepatology 78 (2), 649–669 (2023).
95. Yasmeen, R., Reichert B., Deiuliis J., et al.: Autocrine function of aldehyde dehydrogenase 1 as a determinant of diet- and sex-specific differences in visceral adiposity. Diabetes 62 (1), 124–136 (2013).
96. Qian, F., Sun J., Cao D., et al.: Experimental and Modelling Study of the Denaturation of Milk Protein by Heat Treatment. Korean J Food Sci Anim Resour 37 (1), 44–51 (2017).
97. Hackshaw, K.V., Yao S., Bao H., et al.: Metabolic Fingerprinting for the Diagnosis of Clinically Similar Long COVID and Fibromyalgia Using a Portable FT-MIR Spectroscopic Combined with Chemometrics. Biomedicines 11 (10), (2023).
98. Wan, Y., Li X., Slevin E., et al.: Endothelial dysfunction in pathological processes of chronic liver disease during aging. FASEB J 36 (1), e22125 (2022).
1.